25

Energetics of the Citric Acid Cycle in the Deep Biosphere

Peter A. Canovas, III[1,2] and Everett L. Shock[1,2,3,4]

ABSTRACT

Constraints on the internal composition of microbial cells are used together with standard state thermodynamic data to evaluate energy demands associated with the citric acid cycle and its individual steps to explore geobiochemical processes in the deep subsurface biosphere. Two pressure-temperature ranges are considered: up to 200 °C and to ~2 kb with the revised Helgeson-Kirkham-Flowers equations of state, and up to 200 °C from 10 to 60 kilobars with the Deep Earth Water model. The former pressure-temperature ranges encompass conditions for known life in natural systems, and the latter push the upper pressures for life into those of subduction zones using guidance from laboratory experiments. The neutral solutes H_2(aq) and CO_2(aq) can diffuse freely across cell membranes and impose external conditions into the composition of microbial cells, and as a result there is a range of chemical affinities for citric acid cycle reactions that prevail throughout the deep subsurface biosphere. These ranges raise the possibility that the citric acid cycle releases energy when run in either the forward or reverse directions depending on the affinities involved. The results of this theoretical study support the notion that life may extend far deeper into subduction zones than is generally appreciated.

25.1. PHYSICAL CONDITIONS OF THE DEEP BIOSPHERE

It is estimated that 10%–33% of the total number of living cells on Earth reside within the subsurface deep biosphere on the continents and in the seafloor (Colman et al., 2017; Hoshino & Inagaki, 2019; Inagaki et al., 2015; Ino et al., 2016; Kallmeyer et al., 2012; Magnabosco et al., 2018; Trembath-Reichert et al., 2017; Whitman et al., 1998). These estimates are limited by sampling, which means we are still just beginning to explore the extent, biodiversity, and potential for novel metabolic pathways in the deep biosphere. Our goal is to assist that exploration by providing a geochemical framework for integrating the deep biosphere into geologic processes to facilitate predictions. One way to approach this goal is to determine energetic demands of biochemical pathways and cycles that are met in the deep biosphere by geochemical energy sources. In this chapter, we combine our standard state thermodynamic data for aqueous species involved in the citric acid cycle (Canovas & Shock, 2016) with estimates of their intercellular abundances to evaluate thermodynamic affinities for reactions within the citric acid cycle at elevated pressures and temperatures. We also evaluate new parameters for the same aqueous species consistent with the Deep Earth Water (DEW) model (Sverjensky, Harrison, et al., 2014), which allows us to extrapolate the energetics of the citric acid cycle into conditions of shallow subduction zones. At present, there are no data to indicate that shallow portions of subduction zones are populated with microbes, but existing field and laboratory data indicate that temperatures and pressures in these systems are not necessarily inhibitory for life. We propose that shallow reaches of subduction zones represent the deepest habitats of the deep biosphere.

[1] *School of Earth and Space Exploration, Arizona State University, Tempe, Arizona, USA*

[2] *Group Exploring Organic Processes in Geochemistry (GEOPIG), Arizona State University, Tempe, Arizona, USA*

[3] *School of Molecular Sciences, Arizona State University, Tempe, Arizona, USA*

[4] *Center for Fundamental and Applied Microbiomics, Arizona State University, Tempe, Arizona, USA*

Carbon in Earth's Interior, Geophysical Monograph 249, First Edition. Edited by Craig E. Manning, Jung-Fu Lin, and Wendy L. Mao.

Abundant evidence suggests that extant microbial communities inhabit the subsurface to depths of at least 5 km with well-documented microbial communities flourishing at 4.2 km beneath the Earth's surface (Figure 25.1). Microbes are known to thrive at temperatures in excess of 100 °C at elevated pressures, and at least one strain lives at 121 °C (Takai et al., 2008). These results are summarized in Figure 25.1a, together with conversions of depth to pressure (Figure 25.1b), high-pressure evidence from lab experiments (Figure 25.1c), and the pressure-temperature framework of the present study (Figure 25.1d). Although not all reported depths can be converted to pressures owing to incomplete information in primary sources, many pressures can be estimated for the deep biosphere, and pressures used in laboratory microbial growth experiments extend well beyond those of currently explored subsurface habitats.

Depths and temperatures reported for subsurface samples of microbial life are summarized in Figure 25.1a, which also shows trajectories of crustal geothermal gradients appropriate for continental (a.k.a. terrestrial, 20 °C km^{-1}), oceanic (a.k.a. marine, 35 °C km^{-1}), and hydrothermal (100 °C km^{-1}) settings. Note that some temperatures where subsurface life thrives are <0 °C. While depth may be a physical barrier for microbes to overcome, it is not necessarily a physiochemical barrier. Therefore, pressures were estimated from depths for those cases where sufficient data were reported, as plotted in Figure 25.1b.

Studies of marine sediment and rock samples often include a seawater depth, which we converted to pressure, assuming that a 10.3 m column of seawater would exert 1 atm or 1.013 bar pressure. For terrestrial (continental) samples, pressure was calculated as overburden using either lithostatic or hydrostatic pressure, whichever was appropriate for the system. Overburden (P_{ob}, in Pa) was calculated as

$$P_{ob} = \rho * g * d, \tag{25.1}$$

where ρ represents density in kg m^{-3}, g indicates the gravitational constant 9.806 m s^{-2}, and d stands for the depth in meters. Equation (25.1) provides a close estimate of the pressure beyond that which the atmosphere is exerting on a sample at depth. If the density of a particular rock type was unavailable for a sampling site from literature sources, an estimated average density was used (i.e. 2.65 g cm^{-3} for granite, 2.55 g cm^{-3} for sandstone, and 0.92 g cm^{-3} for ice, etc.). Additional estimates were needed for in situ down-borehole pressures for some groundwater sample locations if the available information was limited to the depth and the artesian head. As an example, one sampling site came from a depth of 1270 m from an artesian well with a head of 466 ft or ~142 m, indicating the ability of the well pressure to sustain a column of water 142 m above the surface, and making the total pressure at the sampling locale that of a column of water under hydrostatic pressure with an apparent depth of 1412 m plus one bar of atmospheric pressure at that location or a total of ~140 bars.

Laboratory experiments confirming microbial growth summarized from the literature shown in Figure 25.1c were conducted at temperatures and pressures throughout and beyond those reached in known subsurface habitats. Presently, laboratory experiments show that microbes are capable of persisting to somewhat higher temperatures than where they are found in nature, as indicated by the highest temperatures in Figure 25.1c. Researchers have also shown that microbes can survive and thrive at pressures of tens of kilobars, which are considerably higher than those known from natural systems. These pressures are reached at several tens of kilometers and suggest that the deep biosphere may extend much deeper than previously thought.

Field and laboratory evidence depicted in Figures 25.1 a–c allows the pressure-temperature (P-T) reference frame for the deep biosphere shown in Figure 25.1d, in which all known habitable P-T space is encompassed in the gray zone. In the study summarized here, we extended the temperature range to 200 °C and pressures to 60 kilobars (6 GPa) to be inclusive. As shown in Figure 25.1d, it is not presently possible to conduct theoretical calculations over all of this P-T space, and the results shown below are truncated by the vapor-liquid saturation (boiling) curve for H_2O at low pressures and high temperatures, and by the liquid-ice phase boundary at high pressures and low temperatures.

We tackled thermodynamic calculations for the citric acid cycle in two stages. First, we assessed chemical affinities for the overall cycle and its component reactions at temperatures and pressures covered by the revised Helgeson-Kirkham-Flowers (HKF) equation of state (Shock et al., 1992), which permits calculations to 5 kb (0.5 GPa). Second, higher pressure calculations were accomplished by estimating an additional set of revised-HKF parameters for the DEW model (Sverjensky, Harrison, et al., 2014), and then completing the extrapolation of chemical affinities to higher pressures. These developments are described below, after the following discussion of the thermodynamic framework employed.

25.2. THERMODYNAMIC FRAMEWORK AND COMPUTATIONAL METHODS

A first step in assessing the thermodynamic viability of a process in the citric acid cycle is to calculate the standard Gibbs energy, ΔG_r^o, of the reactions involved, which relate to the equilibrium constants, K_r, via

$$\Delta G_r^o \equiv -RT \ln K_r, \tag{25.2}$$

where R represents the gas constant and T stands for temperature in Kelvin. Both standard Gibbs energies and

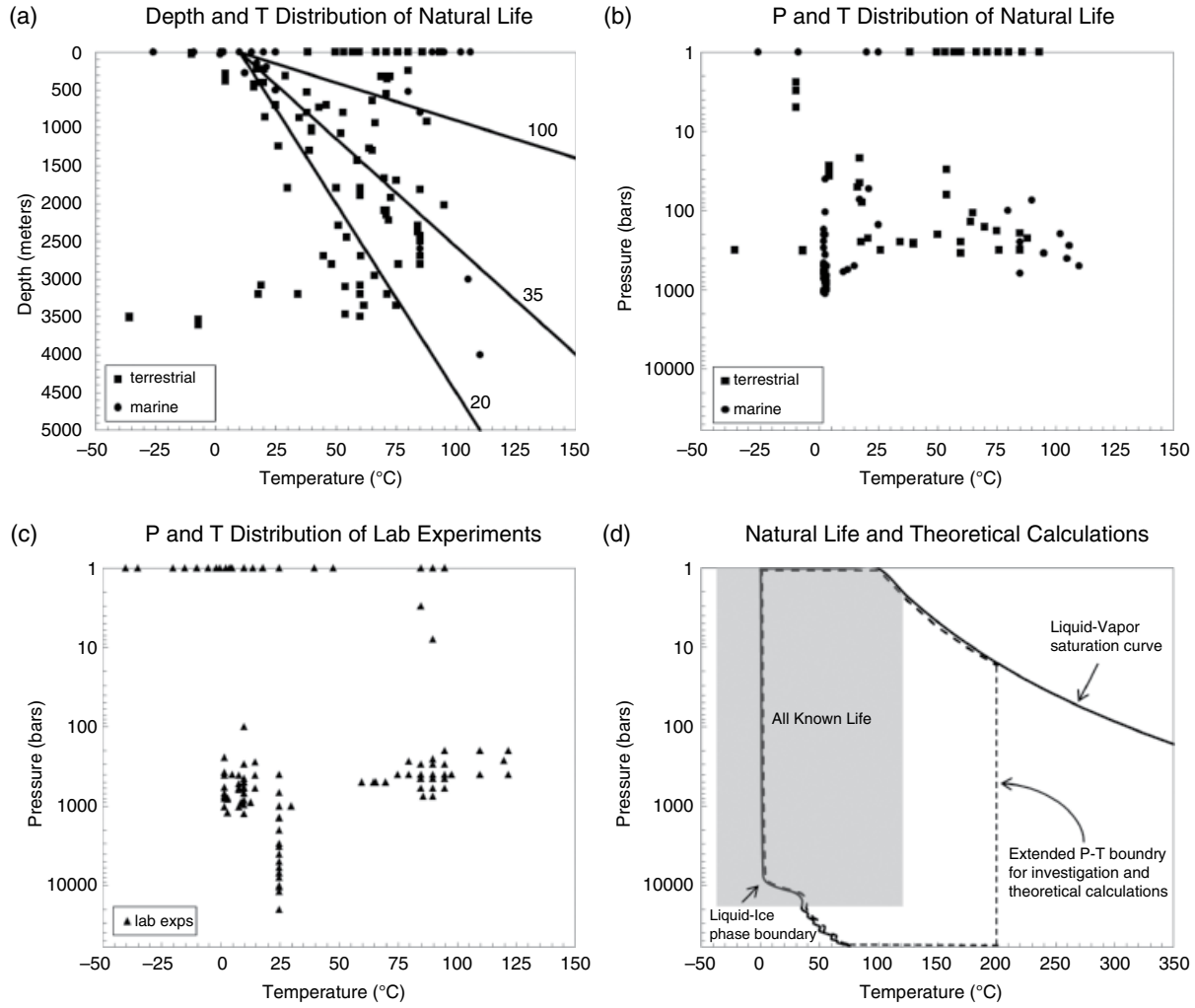

Figure 25.1 The known extent of the Earth's biosphere in depth, temperature, and pressure using evidence from natural systems and laboratory experiments, together with the ranges of thermodynamic calculations conducted in this study. (A) Subsurface habitats and geothermal gradients (in °C km^{-1}) with symbols showing the depths (excluding that of seawater) and temperatures of subsurface samples. Note that geotherms are populated to 4 km depth. (B) Result of converting depths from (A) into pressure, as possible. Many reported depths had no readily available pressure data correlated with them. Our inability to estimate pressures means that several samples shown in (A) were left out of (B). (C) Results of microbial growth laboratory experiments at elevated temperatures and pressures. Note that ranges of temperature and pressure in (C) exceed those in (B). (D) The temperature and pressure ranges of calculations conducted in this study (dashed lines), which encompass most of those established by studies of natural systems and laboratory experiments (gray zone). References for data and pressure estimates include Amend and Shock (2001), Apps (2010), Arcuri and Ehrlich (1977), Ask et al. (2001), Bakermans et al. (2006), Bale et al. (1997), Bartlett (2002), Bernhardt et al. (1988), Bonch-Osmolovskaya et al. (2003), Böning et al. (2004), Brazelton and Baross (2009), Breezee et al. (2004), Byers et al. (1998), Canganella et al. (1997), Carvalho (2013), Chivian et al (2008), Collins et al. (2010), D'Elia et al. (2008), Daumas et al. (1986, 1988), DeLong et al. (1997), Delwiche et al. (1996), Deming and Baross (1986), Deming et al. (1988), Ehrlich et al. (1972), Ekendahl and Pedersen (1994), Ellis and Ege (1975), Erauso et al. (1993), Fardeau et al. (2000), Fell (1967), Grabowski et al. (2005), Greene et al. (1997), Grossman and Shulman (1995), Haldeman et al. (1993), Havig et al. (2011), Inagaki et al. (2003), Johnson et al. (1992), Kaksonen, Plumb, et al. (2006), Kaksonen, Spring, et al. (2006), Kato et al. (1995, 1996, 1997, 1998), Kieft et al. (1999, 2005), Kimura et al. (2005), Klouche et al. (2007), Kotelnikova and Pedersen (1998), Kotelnikova et al. (1998), Kotlar et al. (2011), L'Haridon et al. (1995), H. Li et al. (2006, 2007), X. Li et al. (2010), Liesack et al. (1991), Liu et al. (1997), Loiacono et al. (2012), Love et al. (1993), Marteinsson et al. (1997, 1999, 2013), Meersman et al. (2013), Meyer-Dombard et al. (2011), Miller et al. (1988), Miyoshi et al. (2005), Mochimaru et al. (2007), Mori et al. (2002), Morita and ZoBell (1955), Motamedi and Pedersen (1998), Nakai et al. (2011), Nazina et al. (2007), Nilsen and Torsvik (1996), Nilsen, Torsvik, et al. (1996), Nilsen, Beeder et al. (1996), Nogi et al. (1998), Nunoura et al. (2005), Olson et al. (1981), Onstott et al. (1997, 1998), Panikov and Sizova (2007), Parkes et al. (1994), Pedersen (1997), Pedersen and Ekendahl (1990), Pope et al. (1975), Price and Sowers (2004), Rivkina et al. (2000), Rosnes et al. (1991), Russell et al. (1994), Sahl et al. (2008), Salamatin et al. (1998), Salisbury et al. (2002), Schippers and Neretin (2006), Scholander et al. (1965), Schwarz and Colwell (1975a, 1975b), Schwarz et al. (1975), Sharma et al. (2002), Shi et al. (1997), Shock (2009), Stetter et al. (1993), Steurer and Underwood (2003), Stevens et al. (1993), Stevens and McKinley (1995), Szewzyk et al. (1994, 1997), Takai, Moser, Onstott, et al. (2001), Takai, Moser, DeFlaun, et al. (2001), Takai et al. (2002, 2005, 2008), Tanaka et al. (2001), Tardy-Jacquenod et al. (1998), Tobal (1993), Trimarco et al. (2006), Turley (2000), Vanlint et al. (2011), Wanger et al. (2012), Winnock and Pontalier (1970), Wouters et al. (2013), Wynter et al. (1996), Yanagibayashi et al. (1999), Yayanos et al. (1981, 1982), Yayanos and Dietz (1982), Yayanos (1986), Yoshioka et al. (2009), Zhang et al. (2005, 2006), Zimov et al. (2006), Zink et al. (2003), ZoBell (1952, 1958), and ZoBell and Morita (1957). See electronic version for color representation of the figures in this book.

equilibrium constants are functions of temperature, pressure, and choice of standard state.* The overall Gibbs energy of a reaction, ΔG_r, can be calculated from

$$\Delta G_r = \Delta G_r^o + RT\,ln Q_r, \tag{25.3}$$

where Q_r stands for the activity product given by

$$Q_r = \prod_i a_i^{v_{i,r}}, \tag{25.4}$$

where a_i stands for the activity of the ith chemical species in the reaction and $v_{i,r}$ stands for the stoichiometric reaction coefficient of the ith chemical species in the rth reaction, which is positive for products and negative for reactants.

The overall Gibbs energy change of a chemical system (ΔG) depends on the progress of the various reactions possible in that system. Focusing on individual reactions is facilitated by evaluating their chemical affinities, A_r, defined as

$$A_r \equiv -\left(\frac{\partial \Delta G}{\partial \xi_r}\right)_{P,T,\xi_k}, \tag{25.5}$$

where ξ_r represents the progress of the rth reaction of interest and ξ_k stands for the progress of all other reactions in the system (Helgeson, 1979). According to equation (25.5), as a reaction proceeds and lowers the Gibbs energy of the system, its chemical affinity will be positive and reach zero at equilibrium. Negative affinity values mean that the reverse reaction is favored to proceed. The above relations can be combined to yield

$$A_r = RT\,ln\left(\frac{K_r}{Q_r}\right). \tag{25.6}$$

In practice, we evaluate equilibrium constants for reactions in the citric acid cycle with equations, data, and parameters from Canovas and Shock (2016), together with a new set of parameters developed in this study for the DEW model. Activity products are calculated from compositional constraints from natural or laboratory systems. In the present study, we used this approach to evaulate thermodynamic drives (a.k.a. chemical affinities) for individual steps in the citric acid cycle, as well as the overall cycle over ranges of temperature and pressure that prevail in subsurface environments.

*The aqueous solution standard state adopted in this study is a hypothetical one molal solution referenced to infinite dilution at any temperature and pressure. The standard state for gases is the pure gas at any temperature and 1 bar, that for liquid H_2O is the pure liquid at any temperature and pressure, and that for minerals is the pure crystalline solid at any temperature and pressure.

25.3. EVALUATING CHEMICAL AFFINITIES FOR THE CITRIC ACID CYCLE WITHIN MICROBIAL CELLS

Evaluating chemical affinities requires equilibrium constants and activity products, as demonstrated in the preceding discussion. The revised-HKF equations of state together with data and parameters provided by Canovas and Shock (2016) make it possible to estimate standard state thermodynamic data, including equilibrium constants, for species involved in the citric acid cycle as illustrated in Figure 25.2. The stepwise reactions indicated in Figure 25.2 are listed in Box 25.1, together with definitions of abbreviations. Standard Gibbs energies of these reactions are illustrated at elevated temperatures and up to 5 kb by Canovas and Shock (2016). It should be kept in mind that microbial metabolisms sometimes involve reactions as shown in Figure 25.2, and sometimes the reverse of these reactions. The traditional forward direction of the citric acid cycle reflects human metabolism. Also, we have adopted the convention common to biochemistry in which metabolic reactions are written as if involving only the fully dissociated ionic forms of acids and other compounds, which rarely reflects the actual speciation of these compounds at natural conditions whether inside or outside cells (Canovas & Shock, 2016).

In addition to equilibrium constants, activity products are also needed to evaluate chemical affinities, and to do so requires constraints on the abundances of all of the chemical species shown in Figure 25.2 and linked through the reactions listed in Box 25.1. Data for most of these compounds are scarce from natural environments, but many of their concentrations are constrained within microbial cells. However, these constraints are chiefly from *Escherichia coli* and not from any of the thermophiles or barophiles that thrive in the deep biosphere. Nevertheless, assuming that data from microbes provide better constraints than setting values to arbitrary ranges, we have adopted the data listed in Table 25.1 for the purpose of estimating a set of chemical affinities for the citric acid cycle within cells throughout the deep biosphere. Note that we list these values as apparent activities, as a reminder that we have yet to conduct a comprehensive speciation of these and other solutes within microbial cells. When that becomes possible, and when a greater variety of solute concentrations are obtained on a wider variety of organisms through advances in metabolomics, improvements in the calculated affinities of metabolic processes can be anticipated.

A few notes about the data in Table 25.1 are warranted. As indicated, most of these values come from studies of *Escherichia coli*, which is one of the most thoroughly studied bacteria and from which much has been learned about microbial metabolism and biochemical pathways. Nevertheless, we expect that additional investigations

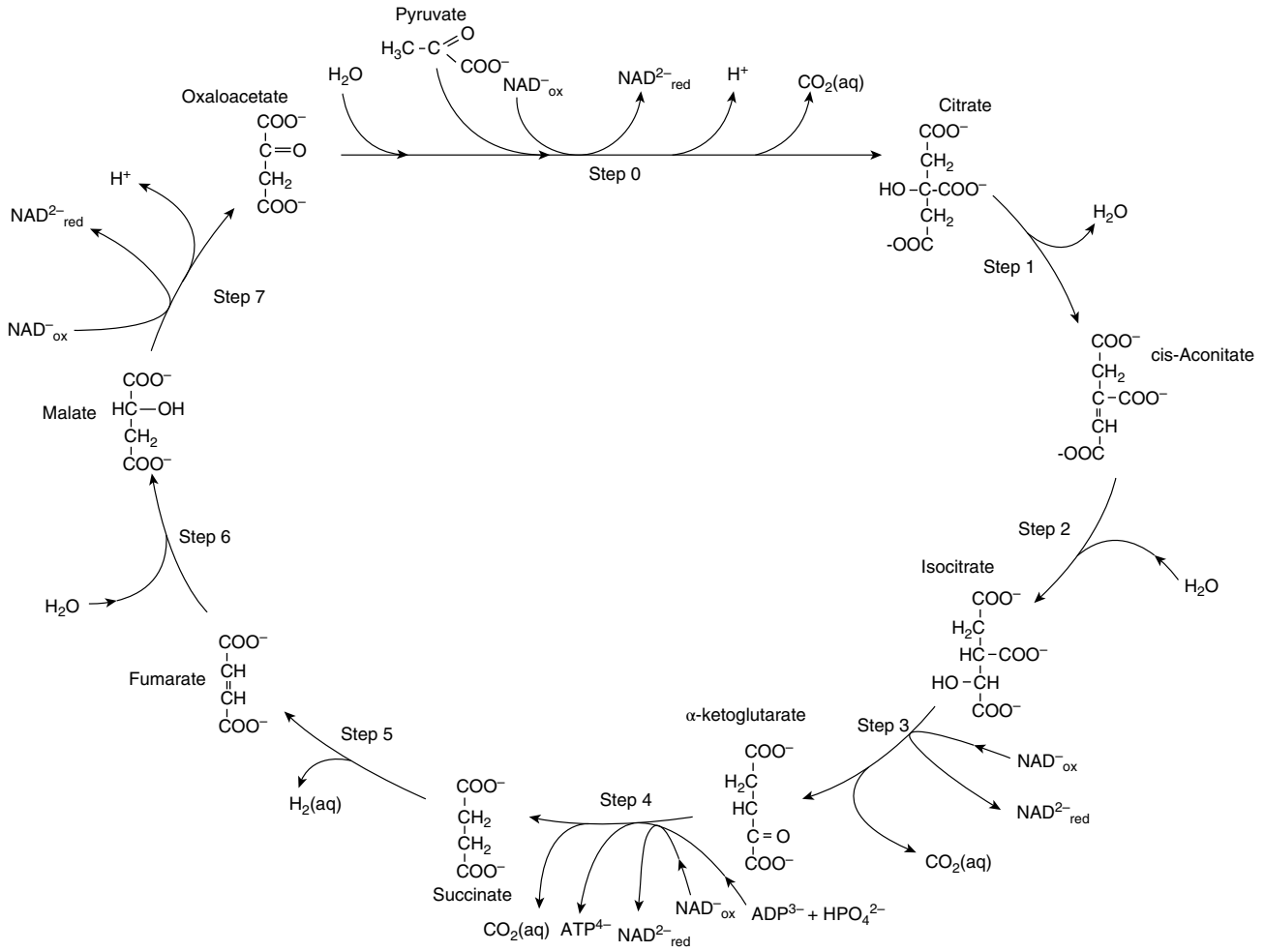

Figure 25.2 (after Canovas & Shock, 2016) Thermodynamic depiction of the citric acid cycle used to assess affinities associated with individual steps, as well as the affinities for the overall metabolic pathway. Some of the steps represent condensed or alternative versions of reactions given in Box 25.1. See electronic version for color representation of the figures in this book.

would yield variations in the values selected. In the case of HPO_4^{2-}, more than one concentration is reported in the literature, so we allowed its activity to vary between the minimum and maximum values reported in Table 25.1. In contrast, we were unable to find measurements on two solutes that appear repeatedly in the citric acid cycle, H_2(aq) and CO_2(aq). One reason is that neutral solutes diffuse more easily across cellular membranes than do ions, which are typically pumped through special ion channels. We have taken advantage of these properties of neutral solutes to assert that their activities within cells are set by their activities in the external environment. In the case of H_2(aq), we chose a lower value set by the concentration in bottom seawater (McCollom, 2007; Shock & Canovas, 2010), and a higher value set by the concentration in hydrothermal fluid venting at the Rainbow hydrothermal field on the mid-Atlantic ridge (Charlou et al., 2002; Shock & Canovas, 2010). The lower value for CO_2(aq) is again taken from bottom seawater (McCollom, 2007; Shock & Canovas, 2010), while the higher value was measured during active fermentation (Merlin et al., 2003) and therefore has somewhat more to do directly with microbial metabolism.

As an example of how affinities are calculated, consider the reaction for step 3 in the citric acid cycle, given by

$$\text{isocitrate}^{3-} + \text{NAD}^-_{\text{ox}} \Rightarrow \alpha\text{-ketoglutarate}^{2-} + \text{NAD}^{2-}_{\text{red}} + \text{CO}_2\,(\text{aq}). \quad (25.7)$$

The version of equation (25.4) for the activity product of reaction (7), Q_7, corresponds to

$$Q_7 = \frac{\left(a\alpha\text{-ketoglutarate}^{2-}\right)\left(a\ NAD^{2-}_{red}\right)\left(aCO_2(aq)\right)}{\left(aisocitrate^{3-}\right)\left(aNAD^-_{ox}\right)}, \quad (25.8)$$

which can be evaluated with data in Table 25.1 to yield $Q_7 = 10^{-4.45}$ using the minimum activity for CO_2(aq).

Box 25.1 Individual reactions representing forward steps in the citric acid cycle, balanced by mass and charge, as illustrated in Figure 25.2 using the biochemical convention of fully dissociated anions.

1. $citrate^{3-} \rightarrow$ *cis*-$aconitate^{3-} + H_2O$
2. *cis*-$aconitate^{3-} + H_2O \rightarrow isocitrate^{3-}$
3. $isocitrate^{3-} + NAD^-_{ox} \rightarrow \alpha\text{-}ketoglutarate^{2-} + NAD^{2-}_{red} + CO_2(aq)$
4. $\alpha\text{-}ketoglutarate^{2-} + NAD^-_{ox} + ADP^{3-} + HPO_4^{2-} \rightarrow succinate^{2-} + NAD^{2-}_{red} + CO_2(aq) + ATP^{4-}$
   4A. $\alpha\text{-}ketoglutarate^{2-} + CoA + NAD^-_{ox} \rightarrow succinyl\text{-}CoA^- + NAD^{2-}_{red} + CO_2(aq)$
   4B. $succinyl\text{-}CoA^- + ADP^{3-} + HPO_4^{2-} \rightarrow CoA + ATP^{4-} + succinate^{2-}$
5. $succinate^{2-} \rightarrow fumarate^{2-} + H_2(aq)$
   5A. $succinate^{2-} + FAD \rightarrow fumarate^{2-} + FADH_2$
6. $fumarate^{2-} + H_2O \rightarrow malate^{2-}$
7. $malate^{2-} + NAD^-_{ox} \rightarrow oxaloacetate^{2-} + NAD^{2-}_{red} + H^+$
0. $pyruvate^- + NAD^-_{ox} + oxaloacetate^{2-} + H_2O \rightarrow citrate^{3-} + NAD^{2-}_{red} + CO_2(aq) + H^+$
   0A. $pyruvate^- + NAD^-_{ox} + CoA \rightarrow acetyl\text{-}CoA + NAD^{2-}_{red} + CO_2(aq)$
   0B. $acetyl\text{-}CoA + oxaloacetate^{2-} + H_2O \rightarrow citrate^{3-} + CoA + H^+$

Overall forward citric acid cycle resulting in pyruvate oxidation, NAD and FAD reduction, and ATP generation:
$pyruvate^- + 4NAD^-_{ox} + ADP^{3-} + HPO_4^{2-} + 2H_2O + FAD \rightarrow 3CO_2(aq) + 4NAD^{2-}_{red} + 2H^+ + ATP^{4-} + FADH_2$
Substituting reaction (5) for 5A as a proxy for the reduction of FAD, as in Figure 25.4:
$pyruvate^- + 4NAD^-_{ox} + ADP^{3-} + HPO_4^{2-} + 2H_2O \rightarrow 3CO_2(aq) + 4NAD^{2-}_{red} + 2H^+ + ATP^{4-} + H_2(aq)$

acetyl-CoA = acetyl-coenzyme A
ATP = adenosine triphosphate
ADP = adenosine diphosphate
CoA = coenzyme A
FAD = oxidized flavin adenine dinucleotide
$FADH_2$ = reduced flavin adenine dinucleotide
NAD^-_{ox} = oxidized nicotinamide adenine dinucleotide
NAD^{2-}_{red} = reduced nicotinamide adenine dinucleotide

Combining this value for Q_7 in equation (25.6) with values of the equilibrium constant for reaction (7), K_7, calculated with data and parameters from Canovas and Shock (2016) yields the affinities for reaction (7) shown in Figure 25.3 for step 3 of the citric acid cycle.

The contoured plots of affinity in Figure 25.3 show minimum values as calculated using values of $H_2(aq)$, $CO_2(aq)$, and HPO_4^{2-} from Table 25.1, which affect the affinities calculated for steps 0, 3, 4, 5, and the overall cycle. Maximum affinities for these steps using alternate data from Table 25.1 are shown in Figure 25.4. Note that the pressure-temperature diagrams in these figures have inverted pressure axes to allow interpretations of changes with depth downward on the plots. The plots cover temperatures from 0 °C to 200 °C, and pressures up to 2 kb. The contours are labeled in kcal mol^{-1} for the reactions as written in Box 25.1. In the case of the overall reactions, these are the calculated affinities for one complete turn of the forward cycle. One striking feature of the majority of the plots shown in Figures 25.3 and 25.4 is that the affinities of most of the reactions in the citric acid cycle depend little on changes in pressure over the pressure range that encompasses all of the known natural occurrences of microbial life, as indicated in Figure 25.1a. Perhaps a useful assumption for most steps of the citric acid cycle in the known subsurface biosphere is that affinities shift meaningfully with temperature but very little with pressure.

Examination of Figure 25.3 reveals that minimum affinities for step 0, in which pyruvate from outside the cycle and oxaloacetate from inside the cycle are combined with H_2O to form citrate and $CO_2(aq)$ coupled with reduction of NAD (nicotinamide adenine dinucleotide), are positive and decrease with increasing temperature at all pressures considered. Positive values of affinity mean that energy would be released as the reaction proceeds as written. Small positive values of affinity are associated with the dehydration of citrate to form *cis*-aconitate in step 1, and they become slightly more positive as temperature increases at all pressures. In contrast, the hydration of *cis*-aconitate to form isocitrate in step 2 is accompanied by small negative affinities that become increasingly negative with increasing temperatures. The results obtained here indicate that this step requires the input of energy throughout the biosphere. Minimum values of affinity for step 3 shown in Figure 25.3, and given by reaction (7) above, are positive and approximately twice the magnitude of the minimum affinities for step 1. Apparently, the oxidative decarboxylation of isocitrate to yield α-ketoglutarate and $CO_2(aq)$, which is coupled to the reduction of NAD, can be an energy-yielding process

Table 25.1 Chemical species in and associated with the citric acid cycle and their apparent activities within microbial cells used in the present study (see text).

Chemical Species	Apparent Activity
$citrate^{-3}$	$2 * 10^{-3}$[a]
$cis\text{-}aconitate^{-3}$	$1.6 * 10^{-5}$[a]
$isocitrate^{-3}$	$2 * 10^{-3}$[b]
$\alpha\text{-}ketoglutarate^{-2}$	$4.4 * 10^{-4}$[a]
$succinate^{-2}$	$5.7 * 10^{-4}$[a]
$fumarate^{-2}$	$1.2 * 10^{-4}$[a]
$malate^{-2}$	$1.7 * 10^{-3}$[a]
$oxaloacetate^{-2}$	$3 * 10^{-5}$[c]
$pyruvate^{-}$	$9 * 10^{-4}$[d]
NAD^{-}_{ox}	$2.6 * 10^{-3}$[a]
NAD^{-2}_{red}	$8.3 * 10^{-3}$[a]
ADP^{-3}	$5.6 * 10^{-4}$[a]
ATP^{-4}	$9.6 * 10^{-3}$[a]
FAD	$1.7 * 10^{-4}$[a]
$FADH_2$	$3.8 * 10^{-5}$[e]
$H_2(aq)$	$1.6 * 10^{-2}$ ($4 * 10^{-10}$)[f]
$CO_2(aq)$	$2 * 10^{-2}$ ($4.93 * 10^{-5}$)[g]
HPO_4^{-2}	$5 * 10^{-3}$ ($2 * 10^{-2}$)[h]
H^+	$1 * 10^{-7}$[i]
H_2O	1[j]

[a] Bennett et al. (2009)

[b] Set equal to that of citrate because no in situ measurement is available

[c] Peng et al. (2004)

[d] Sundararaj et al. (2004) and Phillips et al. (2008)

[e] Ishii et al. (2007)

[f] There are no measurements, but easily diffuses across membranes, and intracellular concentration and apparent activity are assumed to mimic that of the extracellular environment (see text). Value without parentheses corresponds to the dissolved hydrogen concentration from vent fluid at the Rainbow hydrothermal field from Charlou et al. (2002), while the value in parentheses corresponds to that of bottom seawater from McCollom (2007).

[g] Value without parentheses was measured by Merlin et al. (2003) during active fermentation and is used as the value that provides the lowest calculated apparent affinity, while that in parentheses corresponds to the concentration of $CO_2(aq)$ of bottom seawater and therefore aligns with statement by Lu et al. (2009) that the internal $CO_2(aq)$ concentration of cells is essentially that of the external environment.

[h] The value outside of the parentheses corresponds to the concentration from Sundararaj et al. (2004) and Phillips et al. (2008) and provides the lowest calculated apparent affinity, while that in parentheses is the value assumed by Bennett et al. (2009).

[i] Set to neutrality at 25 °C and 1 bar to simplify the calculations, though it should be noted that neutrality depends on temperature and pressure.

[j] Set to unity to simplify the calculations, though it should be noted that the actual activity of water could deviate from this value depending on salinity.

throughout the known biosphere. Minimum affinity contours for step 4 are shaped differently than contours for all other steps in the citric acid cycle, revealing a broad shallow trough of small positive values in pressure and temperature associated with the conversion of α-ketoglutarate to succinate and $CO_2(aq)$ coupled to production of adenosine triphosphate (ATP) from adenosine diphosphate (ADP) and reduction of NAD. The positive values of affinity for steps 3 and 4 are consistent with the notion that the $CO_2(aq)$-producing steps of the forward citric acid cycle are associated with energy release coupled to biosynthesis. In contrast, step 5, in which succinate is oxidized to form the double bond in fumarate, is energetically costly, as revealed by the negative values of affinity at all temperatures and pressures shown in Figure 25.3. However, these results show that the energetic cost of this step decreases with increasing temperature. The hydration of fumarate to malate in step 6 requires energy as indicated by the negative affinity values at all temperatures and pressures, but the magnitudes are much lower than those associated with step 5. Note that the energy cost of step 6 is predicted to increase slightly with increasing temperature at all pressures. The only step in the citric acid cycle that exhibits a change in the sign of its affinity is step 7, in which malate oxidation to oxaloacetate is coupled to NAD reduction. Step 7 requires the input of energy at low temperatures, is accompanied by a release of energy at high temperatures, and is predicted to be the least pressure-dependent of all of the affinities shown in Figure 25.3.

Finally, the plot in the lower right-hand corner of Figure 25.3 shows minimum affinities for the overall forward citric acid cycle in which pyruvate is oxidized to $CO_2(aq)$ and coupled to the reduction of NAD and production of ATP. The minimum affinity values shown for the other steps combine to yield contours that are closely spaced at high temperature and approach an increasingly flat plateau as temperatures decrease, suggesting that energy from the overall citric acid cycle at low temperatures is nearly independent of pressure. They also yield the surprising result that the affinity for the overall forward cycle can be negative at low temperatures and positive at high temperatures while having only a slight pressure dependence. This implies that the citric acid cycle run in reverse would release energy at temperatures below 100 °C at all pressures when using minimum affinity values. Portions of the reverse citric acid cycle are often recognized as aspects of microbial metabolism, and results shown in Figure 25.3 are consistent with the *release of energy* during CO_2 fixation into larger organic compounds via the citric acid cycle under these conditions. This combination of CO_2 fixation into organic forms with the release of energy is an example of how biochemical cycles may have emerged from geochemical precursors (Shock & Boyd, 2015).

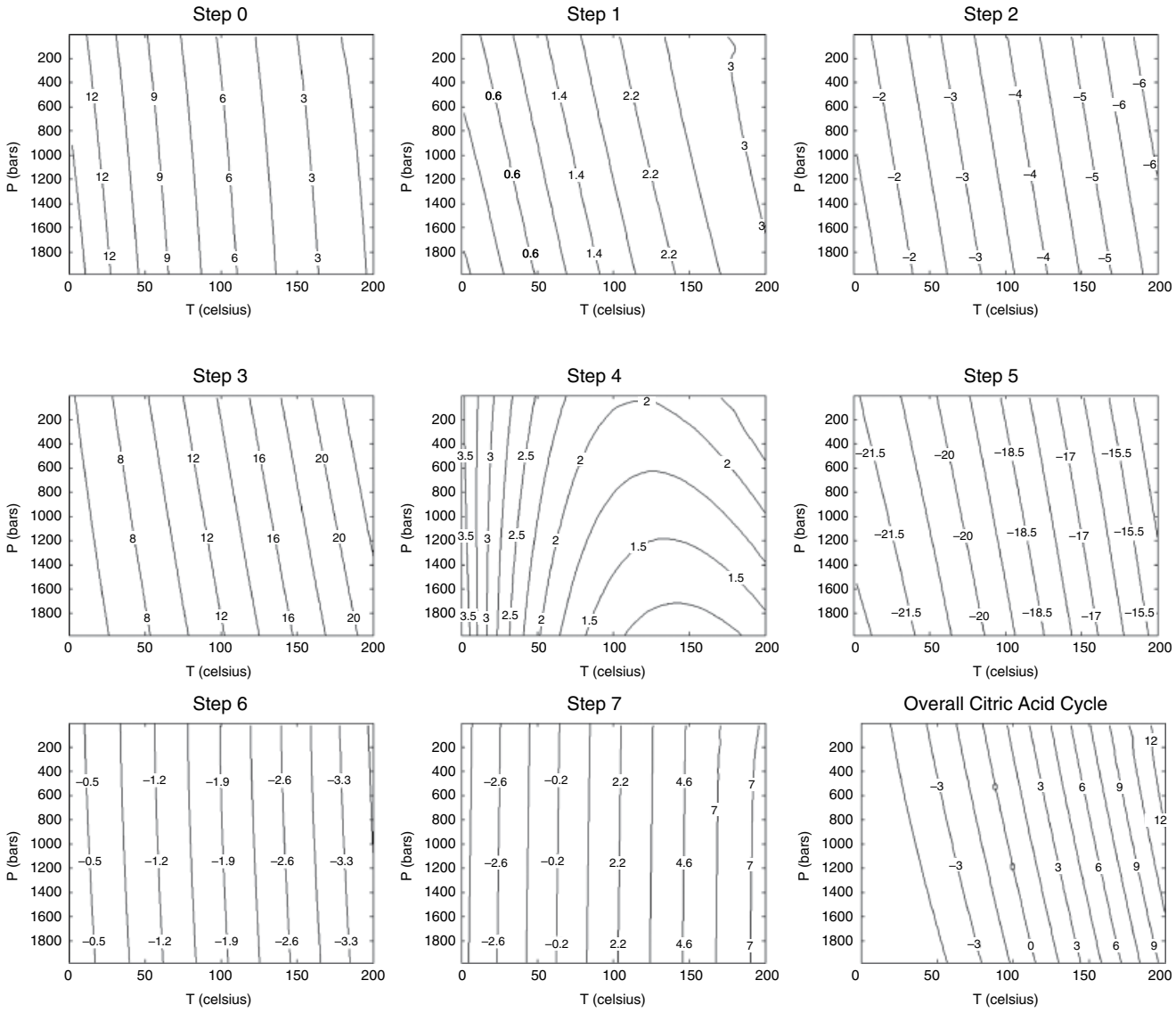

Figure 25.3 Contours of minimum affinity values (in kcal mol^{-1}) as functions of temperature and pressure for steps in the citric acid cycle as given in Box 25.1 and calculated with equation (25.6) using the compositional data listed in Table 25.1 and equilibrium constants calculated with equations, data, and parameters from Canovas and Shock (2016). See electronic version for color representation of the figures in this book.

The notion that the overall forward citric acid cycle would cost energy to run is at odds with its role in human metabolism, but it must be kept in mind that the minimum affinity values from *Escherichia coli* and geochemical constraints used to generate the plot in Figure 25.3 are unlikely to correspond to conditions within human cells. In fact, the notion of the overall forward cycle costing energy at environmental conditions may be challenged by the maximum affinity values shown in Figure 25.4. As mentioned above, steps 0, 3, 4, and 5 all involve either CO_2(aq) or H_2(aq) that can diffuse freely across microbial membranes and impose external environmental conditions inside cells. The plots for these steps in Figure 25.4 reflect the maximum affinities enabled by the ranges of values shown in Table 25.1. The consequences of external control of CO_2(aq) and H_2(aq) are that affinities for steps 0, 3, and 5 can be about 10 kcal mol^{-1} more positive at the maximum values shown in Figure 25.4. In the case of step 5, which is energetically costly regardless of compositional constraints, maximum affinities are considerably less costly than the minimum values shown in Figure 25.3. Note also that the differently shaped contours for step 4 exhibit considerably more positive, energy-releasing values in Figure 25.4 than in Figure 25.3, and that the trough has shifted to lower temperatures. The combined effects of all of these differences cause the maximum affinities for the overall forward cycle to be large and positive at all temperatures and pressures, as shown in Figure 25.4. If these conditions for H_2(aq) and CO_2(aq) are attained in subsurface environments, then the reverse citric acid cycle would

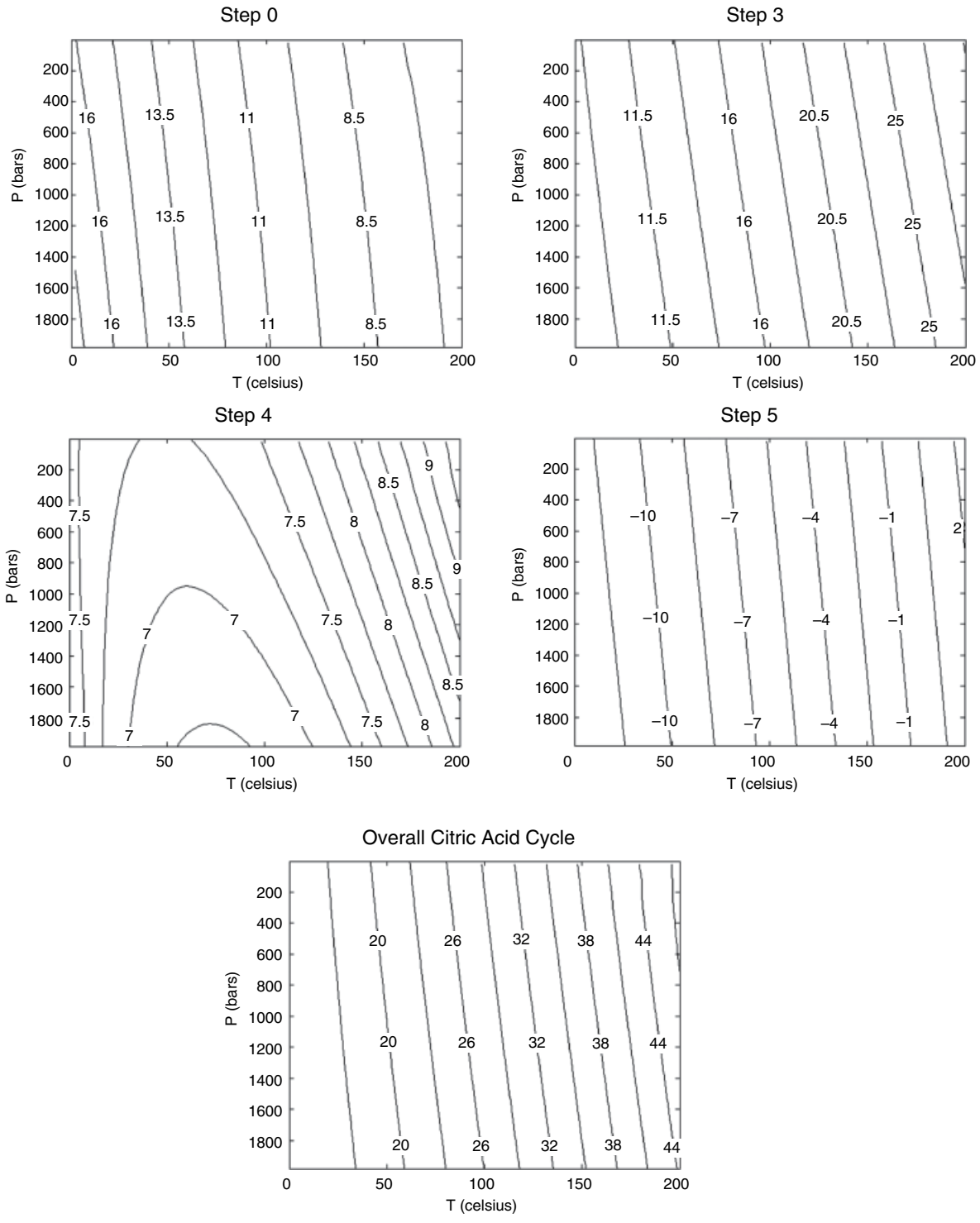

Figure 25.4 Contours of maximum affinity values (in kcal mol^{-1}) as functions of temperature and pressure calculated as in Figure 25.3 for steps in the citric acid cycle affected by variations in H_2(aq), CO_2(aq), and HPO_4^{2-} from Table 25.1. See electronic version for color representation of the figures in this book.

not be a source of energy as it evidently is when minimum affinity values are considered. The consequences of the differences between results in Figures 25.3 and 25.4 underscore the need for development of clever methods to determine solute abundances within microbial cells in laboratory experiments and in natural ecosystems.

25.4. THE CITRIC ACID CYCLE IN A SUBDUCTION ZONE DEEP BIOSPHERE

Does the deep biosphere extend only to the depths we have explored? We doubt it. Laboratory experiments summarized in Figure 25.1c indicate that microbes survive

pressures of tens of kilobars. Coupled with the success of life at temperatures >100 °C, these data suggest a deep biosphere that is far more extensive than revealed by observations of natural systems. Specifically, high pressures and low temperatures found in some subduction zones overlap the conditions of extreme laboratory growth experiments. Based on evidence from these experiments, depths up to 50 km at many continental margins where subduction zones inject cold, altered oceanic crust into the mantle could provide stable and habitable zones where microorganisms could thrive. Habitable depths might be even deeper at fast subduction zones that are also characterized by old, cold slabs with high slab dip angles, such as those occurring at Tonga.

Geophysical models of the relations between depth, pressure, and temperature in the Tonga subduction zone (Syracuse et al., 2010) are shown in Figure 25.5. The warmer slab surface intersects the 121 °C isotherm at about 50 km depth, corresponding to a pressure of about 15 kb in all models. The cooler Moho, which is deeper in the insulated interior of the slab, would intersect the 121 °C isotherm at a little more than 100 km depth and a pressure of about 35 kb. These observations lead to the conclusion that the highest temperatures and pressures of laboratory microbial experiments are attained within the upper 100 km, or so, of the Tonga subduction zone. In this study, we conducted calculations up to 200 °C to include additional conditions where life may thrive in excess of the currently established upper temperature. Note that the slab surface intersects the 200 °C isotherm at about 20 kb in Figure 25.5. The models for conditions at the Moho diverge as temperatures increase and intersect the 200 °C isotherm at pressures from ~44 kb to ~52 kb. These conditions are within the pressure-temperature limits of the DEW geochemical model (Sverjensky, Harrison, et al., 2014), which allows us to calculate standard state thermodynamic data throughout this deepest of potential subsurface biospheres.

The DEW model accounts for experimentally determined properties of water and aqueous solutions to 60 kb (6.0 GPa) and has enabled new perspectives on the progress of water-rock-organic reactions in subduction zone fluids and the upper mantle (Facq et al., 2014; Guild & Shock, 2019; Huang et al., 2017; Sverjensky, Stagno, et al., 2014; Tao et al., 2018). The development of the DEW model is accompanied by changes in how some of the revised-HKF equation of state parameters are estimated. Specifically, extrapolations to high pressures required revision of the way that standard partial molal volumes of aqueous species are calculated with the revised-HKF parameters. Correlation methods provided by Sverjensky, Harrison, et al. (2014) allow estimates of these parameters in the absence of experimental data, which is the case for everything involved in the citric acid cycle other than H^+ and CO_2(aq). These methods were used together with existing standard state data from Canovas and Shock (2016) to obtain the revised-HKF equation of state parameters in Table 25.2 that can be

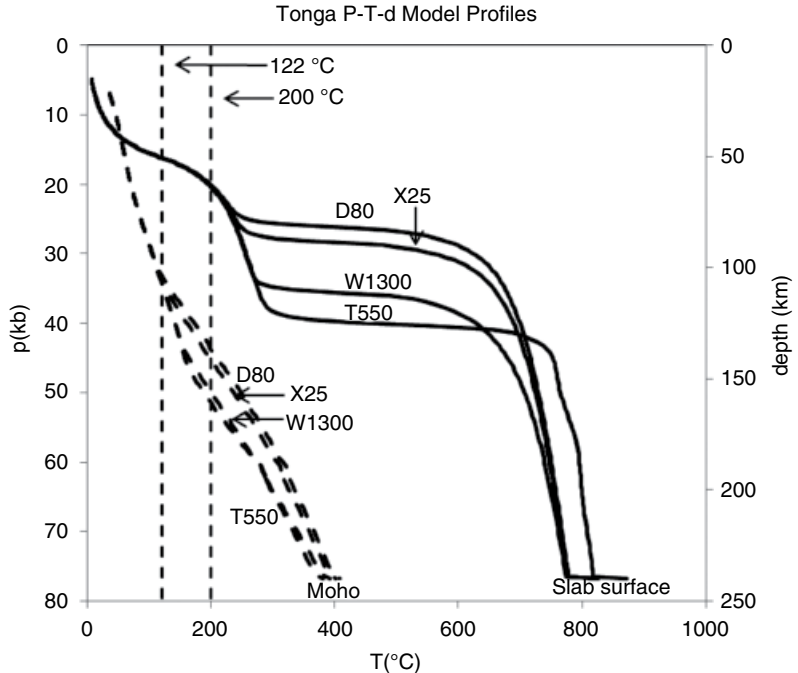

Figure 25.5 Depths, pressures, and temperatures for the slab surface (solid curves) and Moho (~7 km below the slab surface, dashed curves) in the Tonga subduction zone using geothermal gradient modeling data from the D80, T550, W1300, and X25 models of Syracuse et al. (2010). Dashed vertical lines indicate the highest known temperature for life (121 °C), as well as the highest temperature used in citric acid cycle affinity calculations (200 °C). Note that all models of the subduction zone produce depths and pressures that are essentially the same at 121 °C, and that model differences at slightly higher temperatures affect the pressure/depth relations at 200 °C. See electronic version for color representation of the figures in this book.

Table 25.2 Summary of standard partial molal thermodynamic data at 25 °C and 1 bar for aqueous species in the citric acid cycle (Canovas & Shock, 2016) and related biomolecules that take part in reactions in the citric acid cycle (LaRowe & Helgeson, 2006a, 2006b) that are not included in the Deep Earth Water (DEW) database, along with equation of state parameters required to calculate the corresponding properties at high temperatures and pressures between 10 and 60 kb. Unless otherwise indicated, revised-HKF equation of state parameters were estimated using the software from DEW model version 11.0.1 (Sverjensky, Harrison, et al., 2014).

Species	$\Delta\bar{G}_f^{o}$ [a]	$\Delta\bar{H}_f^{o}$ [a]	$\bar{S}^{o}$ [b]	$\bar{C}_p^{o}$ [b]	$\bar{V}^{o}$ [c]	$a_1 \times 10^{1}$ [d]	$a_2 \times 10^{-2}$ [d]	a_3 [e]	$a_4 \times 10^{-4}$ [f]	c_1 [b]	$c_2 \times 10^{-4}$ [f]	$\omega_e \times 10^{-5}$ [a]
Citric acid	−297180.	−364527.	78.89	73.47	112.98	23.4335	18.0278	−10.2781	−3.5243	48.6718	11.9312	−0.06[g]
H_2-citrate$^-$	−292912.	−363530.	67.92	47.04	102.48	22.1425	16.7987	−9.2475	−3.4735	47.5542	6.5474	1.50[g]
H-citrate^{2-}	−286417.	−362947.	48.09	7.71	91.08	20.3986	15.1383	−7.8553	−3.4048	33.5330	−1.4641	2.48[g]
Citrate^{3-}	−277690.	−363750.	16.13	−43.16	74.08	17.2265	12.1182	−5.3229	−3.2800	6.2075	−11.8263	2.75[g]
Cis-aconitic acid	−236200.	−291400.	63.9	64.0	108.7	22.5524	17.1890	−9.5747	−3.4896	42.1636	10.0022	−0.1640[h]
H_2-*cis*-aconitate$^-$	−233600.	−290480.	58.2	37.6	98.2	20.9505	15.6638	−8.2958	−3.4265	35.0910	4.6245	0.7477[h]
H-*cis*-aconitate^{2-}	−227700.	−289900.	40.4	−1.7	86.8	19.6254	14.4022	−7.2380	−3.3744	29.1329	−3.3809	2.6010[h]
Cis-aconitate^{3-}	−218970.	−290700.	8.4	−52.6	69.8	17.3231	12.2102	−5.4000	−3.2838	18.4954	−13.7492	4.6843[h]
Isocitric acid	−295880.	−363960.	76.4	74.5	114.3	23.6793	18.2619	−10.4743	−3.5339	49.0727	12.1411	−0.0820[h]
H_2-isocitrate$^-$	−291390.	−362960.	64.7	48.1	103.8	21.9908	16.6543	−9.1264	−3.4675	40.3381	6.7634	0.6493[h]
H-isocitrate^{2-}	−284960.	−362380.	45.1	8.8	92.4	20.6788	15.4052	−8.0790	−3.4158	34.6306	−1.2420	2.5298[h]
Isocitrate^{3-}	−276230.	−363180.	13.1	−42.1	75.4	18.3766	13.2132	−6.2410	−3.3252	23.9941	−11.6104	4.6132[h]
α-ketoglutaric acid	−201800.	−245700.	76.1	39.9	95.7	20.0660	14.8217	−7.5897	−3.3917	28.7766	5.0930	−0.0840[h]
H-α-ketoglutarate$^-$	−198800.	−242300.	77.1	2.9	88.9	19.0070	13.8134	−6.7443	−3.3500	12.1179	−2.4439	0.4615[h]
α-ketoglutarate^{2-}	−191800.	−240400.	60.1	−49.9	82.7	18.6860	13.5078	−6.4881	−3.3374	−1.8644	−13.1992	2.3026[h]
Succinic acid	−177800.	−218000.	62.3	53.3	82.44	17.4474	12.3285	−5.4993	−3.2887	35.7970	7.8226	−0.1744[h]
H-succinate$^-$	−172060.	−217350.	45.2	9.3	69.99	15.5663	10.5375	−3.9975	−3.2146	20.3194	−1.1402	0.9446[h]
Succinate^{2-}	−164380.	−217350.	19.5	−50.5	56.32	13.8575	8.9105	−2.6333	−3.1474	3.4443	−13.3215	2.9170[h]
Fumaric acid	−154820.	−186260.	60.62	47.00	77.9	16.5601	11.4838	−4.7909	−3.2537	31.9979	6.5393	−0.1860[h]
H-fumarate$^-$	−150600.	−186150.	46.83	10.0	65.4	14.6630	9.6775	−3.2764	−3.1791	20.5021	−0.9976	0.9199[h]
Fumarate^{2-}	−144320.	−186830.	23.48	−42.8	51.7	12.9315	8.0290	−1.8941	−3.1109	7.4061	−11.7530	2.8572[h]
Malic acid	−213530.	−259310.	68.21	56.43	82.22	17.4231	12.3054	−5.4799	−3.2877	37.9851	8.4602	−0.1360[h]
H-malate$^-$	−208810.	−258610.	54.75	19.4	75.40	16.5476	11.4718	−4.7809	−3.2532	24.9065	0.9172	0.8000[h]
Malate^{2-}	−201860.	−258890.	30.48	−33.4	69.19	16.2774	11.2146	−4.5662	−3.2426	11.9385	−9.8382	2.7512[h]
Oxaloacetic acid	−200000.	−235100.	72.9	29.1	79.1	16.8320	11.7426	−5.0080	−3.2644	22.2537	2.8931	−0.1050[h]
H-oxaloacetate$^-$	−196600.	−231300.	74.0	−7.9	72.3	15.8056	10.7654	−4.1886	−3.2240	6.2205	−4.6438	0.5084[h]
Oxaloacetate^{2-}	−190600.	−230300.	57.2	−60.7	66.1	15.4832	10.4584	−3.9312	−3.2114	−7.7894	−15.3992	2.3465[h]

(Continued)

Table 25.2 (Continued)

Species	$\Delta\bar{G}_f^o$ [a]	$\Delta\bar{H}_f^o$ [a]	$\bar{S}^o$ [b]	$\bar{C}_P^o$ [b]	$\bar{V}^o$ [c]	$a_1 \times 10^{1}$ [d]	$a_2 \times 10^{-2}$ [d]	a_3 [e]	$a_4 \times 10^{-4}$ [f]	c_1 [b]	$c_2 \times 10^{-4}$ [f]	$\omega_e \times 10^{-5}$ [a]
Pyruvic acid	−117000.	−140300.	62.1	36.3	64.6	13.9819	9.0291	−2.7327	−3.1523	25.8192	4.3597	−0.1760 [h]
$Pyruvate^-$	−113600.	−137400.	60.4	−3.7	51.5	11.8649	7.0134	−1.0426	−3.0689	10.5798	−3.7883	0.7144 [h]
NAD^{2-}_{red}	−524441.	−783126.	137.2	177.2	335.8	70.7652	63.0924	−48.0643	−5.3872	187.4039	33.0608	8.4 [i]
NAD^-_{ox}	−529811.	−776066.	147.6	169.7	335.9	70.7846	63.1109	−48.0798	−5.3880	183.0056	31.5321	8.4 [i]
ADP^{3-}	−452649.	−624106.	52.17	41.5	191.7	40.6730	34.4416	−24.0408	4.2028	67.3629	5.4271	4.0 [i]
ATP^{4-}	−657038.	−859264.	47.96	21.3	196.8	42.1334	35.8320	−25.2067	−4.2603	64.7373	1.3124	5.0 [i]

[a] cal mol^{-1},
[b] cal mol^{-1} K^{-1},
[c] cm^3 mol^{-1},
[d] cal mol^{-1} bar^{-1},
[e] cal K mol^{-1} bar^{-1},
[f] cal K mol^{-1},
[g] LaRowe and Helgeson (2006a),
[h] Canovas and Shock (2016),
[i] LaRowe and Helgeson (2006b).

used with the DEW model, which already includes H^+, $H_2(aq)$, $CO_2(aq)$, and HPO_4^{2-}. It should be noted that these parameters can be used reliably at pressures between 10 kb and 60 kb, but not below 10 kb.

Equilibrium constants for the reactions in Box 25.1 were calculated with the DEW model for temperatures up to 200 °C and pressures from 10 to 60 kb. At the lower temperatures and higher pressures considered, a polymorph of ice is stable rather than liquid water, so equilibrium constants for reactions involving aqueous solutes were not calculated at these conditions. Values of activity products were calculated as described above using data from Table 25.1 and combined with the DEW-based equilibrium constants to evaluate affinities throughout low-temperature conditions of subduction zone fluids in the Tonga model shown in Figure 25.5. The results are shown in Figure 25.6 for minimum affinity values and in Figure 25.7 for maximum affinity values, using the same constraints as in the construction of Figures 25.3 and 25.4.

The plots in Figure 25.6 show minimum affinity contours on P-T plots that extend from 10 to 60 kb and from 0 °C to 200 °C. These plots also show depths on the right-hand ordinate. The contours are truncated where they hit the edge of the ice stability field. Also shown in each plot are traces of the slab surface (solid curve) and the Moho (dashed curve) from the Tonga subduction models adopted from Figure 25.5. A striking feature of the plots in Figure 25.6 is that the affinity contours have considerably lower slopes than the corresponding low-pressure plots shown in Figure 25.3. In fact, rather than being able to conclude that the minimum affinities for the citric acid cycle and most of its individual steps change with temperature but are nearly independent of pressure, which is the case of the low-pressure predictions, at the higher pressures of Figure 25.6, affinities depend strongly on both pressure and temperature. In several cases, the trajectory of the slab surface in pressure and temperature is roughly parallel with the affinity contours of individual steps, suggesting that slab surface conditions are energetically similar for these reactions regardless of depth. In contrast, the trajectory of the Moho cuts across the affinity contours. The implication is that the energetic consequences for the citric acid cycle at the Moho are considerably more variable than at the slab surface.

Minimum affinities for step 0 in Figure 25.6 are positive and increase with increasing pressure, indicating that this reaction yielding citrate and $CO_2(aq)$ from pyruvate and oxaloacetate is predicted to release energy throughout shallow conditions in steeply dipping subduction zones. Affinities for step 0 at the conditions of the slab surface vary from 17 kcal mol^{-1} at the initiation of subduction to 12 kcal mol^{-1} at 200 °C and depth >60 km, which is equivalent to the affinity at 25 °C and ~1 kb for step 0 in Figure 25.3. In contrast to the subparallel trajectory of the slab surface, the trajectory for the Moho crosses several affinity contours and is consistent with greater energy releases with increasing depth, maximizing at about 29 kcal mol^{-1} at 200 °C and nearly 160 km. Although the slopes of the affinity contours for step 1 are similar to those for step 0, the magnitudes of the affinities are opposite in sign and become more negative with increasing depth and pressure. This means that the dehydration of citrate to form *cis*-aconitate is not favored at these conditions and would require the input of energy. The energy requirements at slab surface conditions are considerably milder than along the trace of the Moho. These results contrast with affinities for step 1 at low pressures shown in Figure 25.3, which are small and positive at all pressures and temperatures considered.

The slab-surface trajectory is also subparallel to the minimum affinity contours for steps 2, 3, and 5 as shown in Figure 25.6. Those for step 2 hover around zero, those for step 3 are slightly negative, and those for step 5 are strongly negative, which means that the hydration of *cis*-aconitate to isocitrate is predicted to effectively break even, the oxidation of isocitrate to α-ketoglutarate and $CO_2(aq)$ requires a small input of energy, and the oxidation of succinate to fumarate is cost intensive. Comparison with analogous plots in Figure 25.3 shows that differences in the magnitudes of affinities between the low-pressure and high-pressure calculations are least for step 2 and considerably more dramatic for steps 3 and 5. The effects of pressure are particularly noteworthy for step 3, as strongly negative affinities can be encountered at subduction zones of Figure 25.6 that are not seen at the lower pressures in Figure 25.3. It should be kept in mind that negative affinities for forward reactions also mean that the reverse reactions would release energy. It is particularly notable that the reduction of fumarate to succinate, the reverse version of step 5, would release considerable energy at slab-surface conditions. The Moho trajectory for step 2 crosses the affinity contours much like it does for steps 0 and 1, and like step 0 becomes more energetically favorable with depth. In contrast, the Moho trajectories for steps 3 and 5, which also cross many affinity contours, extend into conditions where these reactions are increasingly costly with increasing depth. Again, this means that the reverse reactions would be energy releasing, and both are capable of releasing impressive amounts of energy along the Moho trajectory.

The minimum affinity contours shown in Figure 25.6 for steps 4, 6, and 7 are steeper than the trajectories for the other steps, and as a consequence, the changes along slab-surface and Moho trajectories appear to be more dramatic. However, the spacings between contours for steps 4 and 6 are considerably smaller than in the plots for steps 0, 1, 3, and 5, and those for step 7 are comparable to those for step 2. In the case of step 4, in which the

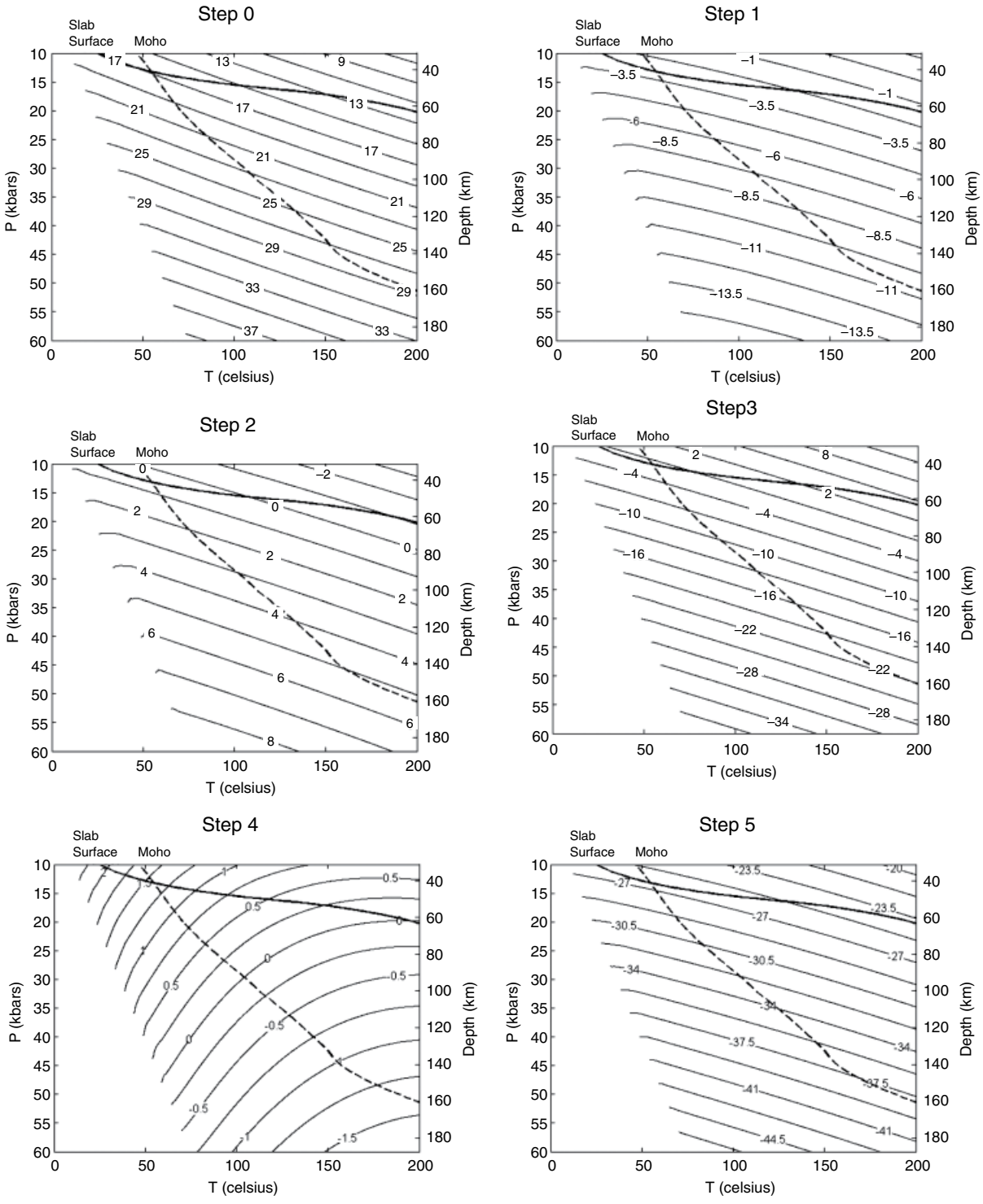

Figure 25.6 Contours of minimum affinity values (in kcal mol^{-1}) as functions of temperature and pressure for steps in the citric acid cycle as given in Box 25.1 and calculated with equation (25.6) using the compositional data listed in Table 25.1 and equilibrium constants calculated with the DEW model using data and parameters from Table 25.2. Slab-surface and Moho trajectories for the Tonga subduction zone shown in Figure 25.5 are indicated. See electronic version for color representation of the figures in this book.

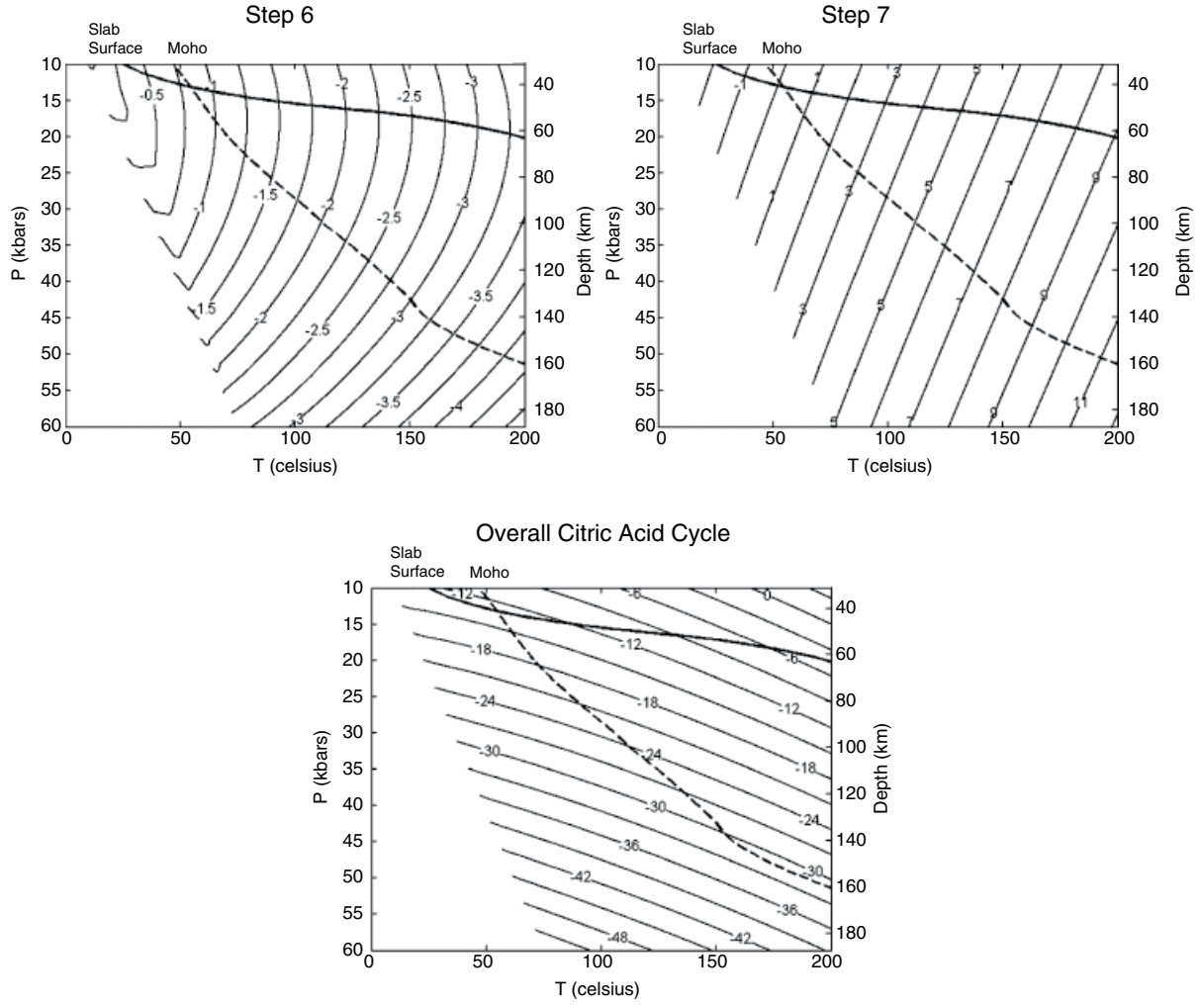

Figure 25.6 (Continued)

oxidation of α-ketoglutarate to succinate and CO_2(aq) is coupled to the production of ATP from ADP, minimum affinities change along the slab surface from slightly positive to zero with increasing depth. The Moho trajectory for step 4 crosses into negative affinity values, consistent with energy release if the reaction were to proceed in the reverse direction of how it is written in Box 25.1, leading to production of α-ketoglutarate. Small positive affinity values accompany step 4 at the lower pressure plots in Figure 25.3 as well. As in the case of step 4, slab-surface and Moho trajectories for step 6 in Figure 25.6 also move to somewhat more negative values with depth, which means that hydration of fumarate to malate becomes increasingly costly, and the reverse reaction more energetically favorable over the course of shallow subduction. Note that the magnitudes of the affinities for step 6 at the high-pressure conditions shown in Figure 25.6 are similar to the those at much lower pressures shown in Figure 25.3. In contrast to the high-pressure behavior shown by step 6, the Moho and slab-surface trajectories for step 7 move to more positive affinities with increasing depth, indicating that the oxidation of malate to oxaloacetate yields increasing energy with depth. The steep contours for step 7 indicate that changes in temperature tend to have more profound effects on the minimum affinities than do changes in pressure, which is a conclusion reached for most steps in the citric acid cycle at low pressures illustrated in Figure 25.3.

Minimum affinity contours for the overall citric acid cycle shown in Figure 25.6 almost all show negative values, indicating that the forward citric acid cycle costs energy and that the reverse citric acid cycle would be capable of releasing energy. The slab-surface trajectory moves to less negative values with increasing depth, but the Moho trajectory moves steadily to more negative values with increasing depth before becoming essentially parallel to the affinity contours at depths greater than

140 km. Note that deep Moho trajectories for steps 0, 1, 2, 3, and 5 also approach constant affinity values at these depths, which is why the overall cycle affinities show this behavior. All subduction zone affinities for the overall cycle in Figure 25.6 are more negative than any of the affinity contours for the overall cycle in Figure 25.3. In terms of minimum affinities, this means that increasing depth increasingly favors the reverse citric acid cycle.

As in the low-pressure examples discussed above, variations in activities of H_2(aq), CO_2(aq), and HPO_4^{2-} from Table 25.1 will affect the affinities of steps 0, 3, 4, and 5, and therefore the affinities of the overall cycle as well. Maximum affinities attainable owing to these activity variations are shown for these steps in Figure 25.7 for high-pressure conditions. Note that affinities for step 0 in Figure 25.7 are about 6 kcal mol^{-1} more positive than in Figure 25.6. Similarly, those for step 3 are about 4 kcal mol^{-1} more positive, and those for step 5 are about 15 kcal mol^{-1} more positive. The curved contours for step 4 fall in somewhat different positions in Figure 25.7 than they do in Figure 25.6, and affinities are generally between 3 and 6 kcal mol^{-1} more positive in Figure 25.7. The consequences of these more positive affinities in the maximum case are dramatic for the affinities of the overall cycle shown in Figure 25.7. Neither the slab-surface nor the Moho trajectories are predicted to cross into negative affinity territory, although the Moho trajectory reaches a broad minimum of about 2 kcal mol^{-1} below about 120 km. In contrast, the slab-surface trajectory is predicted to cross into more and more positive affinity values with depth. Unlike the minimum affinity values shown in Figure 25.6, which are consistent with the reverse citric acid cycle releasing energy throughout shallow subduction conditions, maximum affinity values lead to the prediction that the forward citric acid cycle would release energy. These dramatic differences underscore the influence of changes in the composition of the external geochemical environment on how basic biochemical processes can operate, which can be anticipated from the principles of geobiochemistry (Shock & Boyd, 2015).

The two pressure-temperature ranges described above do not overlap, owing to constraints of the revised-HKF and DEW models, and the vertical axes vary enormously in range. Nevertheless, it is possible to envision how contours connect from the lower pressure plots in Figure 25.3 and 25.4 to the higher pressure plots in Figures 25.6 and 25.7. The nearly vertical contours in Figures 25.3 and 25.4 must bend at higher pressures to become the much flatter contours in Figure 25.6 and 25.7, reflecting the increasing influence of changes in reaction volumes as pressure increases. It is useful to take the scales of the figures into account. As an example, the A_r = –2 kcal mol^{-1} contour toward the left of the step 2 plot in Figure 25.3 has a slope of ~0.125 °C bar^{-1}, and the same A_r = –2 kcal mol^{-1} contour in the upper right corner of the Step 2 plot of Figure 25.6 has a slope of 0.007 °C bar^{-1}. In the eight-kilobar gap between the two figures, this contour apparently moves from <50 °C at 2 kb to ~ 150 °C at 10 kb, with a change in slope of ~95%.

25.5. GEOCHEMICAL INFLUENCE ON THE POTENTIAL ENERGY YIELD OF THE CITRIC ACID CYCLE

In an effort to emphasize how geochemical compositional differences affect the energy yield of the citric acid cycle and even which direction yields energy, we have assembled the four overall citric acid cycle plots from Figures 25.3, 25.4, 26.6, and 25.7 in Figure 25.8 and used color scales to illustrate the differences in affinities. It should be kept in mind that it is the variations in H_2(aq), CO_2(aq), and HPO_4^{2-}, all of which depend on differences in geochemical processes, that drive the differences in affinity ranges in these figures.

The top two plots in Figure 25.8 show affinities for the overall cycle for the minimum case on the left and the maximum case on the right, and both use the same color coding indicated by the upper right bar. Using the same scale allows the observation that the plot for minimum affinity conditions is considerably flatter, varying from about 10 to about −5 kcal mol^{-1}, than the maximum affinity version, in which affinity values range from about 10 to about 45 kcal mol^{-1}. Note that the equilibrium, A_r = 0, contour appears on the minimum affinity plot and not on the maximum affinity plot. It follows that all affinities in the maximum case are positive and consistent with energy release through the citric acid cycle by its operation in the forward direction. In the minimum affinity case, most of the left side of the plot is in negative affinity space, and much of that negative affinity space encompasses the known subsurface biosphere as illustrated in Figure 25.1d. Therefore, this analysis is consistent with the citric acid cycle dominantly operating to release energy in the reverse direction at minimum affinity ranges controlled by geochemical processes in the subsurface.

A similar story is revealed by comparing the minimum and maximum affinity plots for subduction zone pressures and temperatures shown in the lower two plots in Figure 25.8, which use the color coding indicated by the lower right bar. As shown in the plot in the lower right, maximum affinity values are consistent with positive affinities for the overall citric acid cycle throughout conditions attained along the slab-surface and Moho trajectories, although the latter approaches the A_r = 0 contour at the greatest depths. Geochemical compositions leading to these maximum affinity values would be consistent with energy release through the forward citric acid cycle in subduction zone habitats. In contrast, the lower left

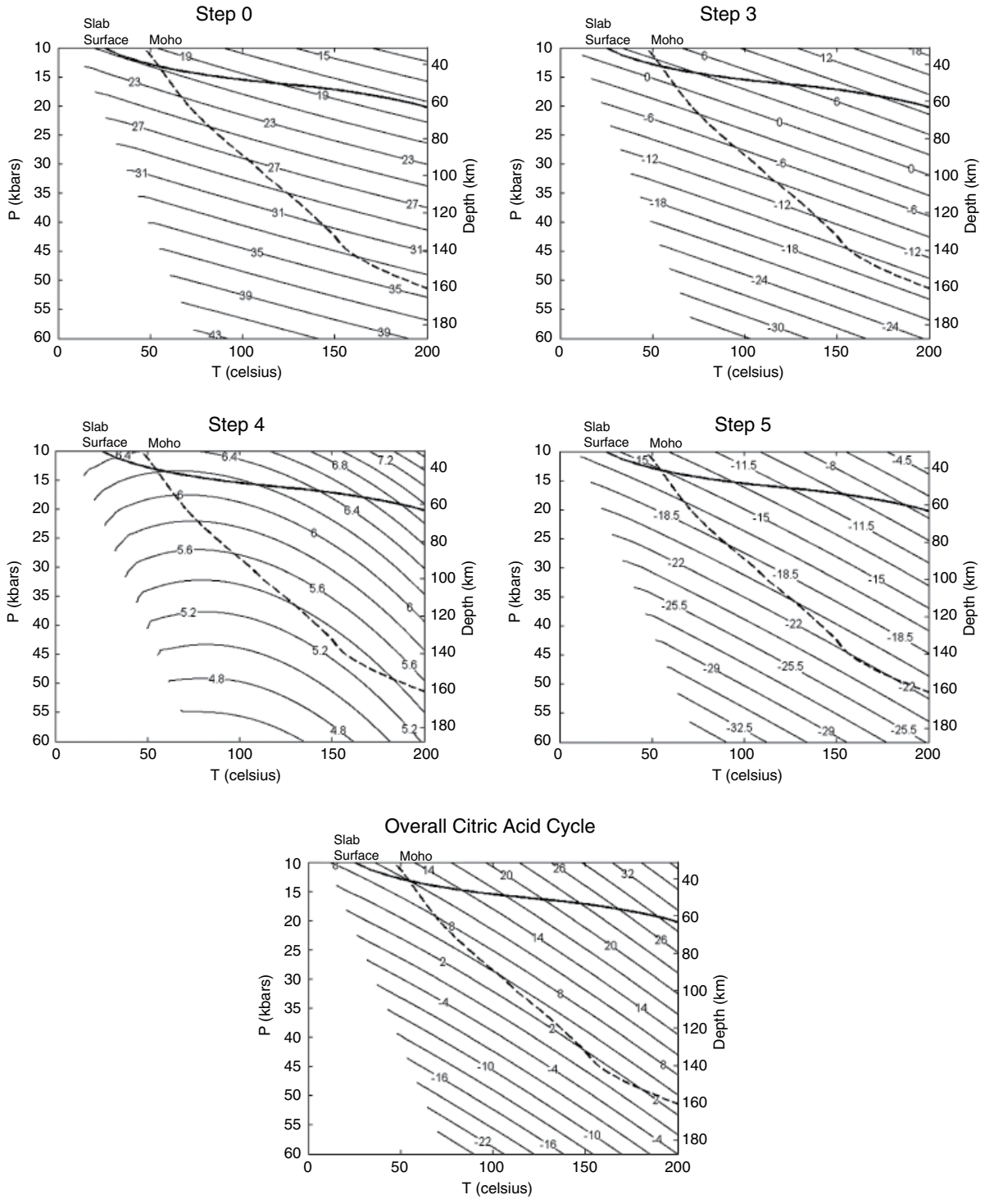

Figure 25.7 Contours of maximum affinity values (in kcal mol^{-1}) as functions of temperature and pressure calculated as in Figure 25.6 for steps in the citric acid cycle affected by variations in H_2(aq), CO_2(aq) and HPO_4^{2-} from Table 25.1. See electronic version for color representation of the figures in this book.

plot indicates that minimum affinity values are consistent with negative affinities over most of the pressures and temperatures considered, which means that the reverse citric acid cycle would be associated with energy release in subduction habitats. In general, conditions along the slab-surface trajectory fall at about −10 kcal mol^{-1}, while those along the Moho trajectory reach −30 kcal mol^{-1} at the greatest depths.

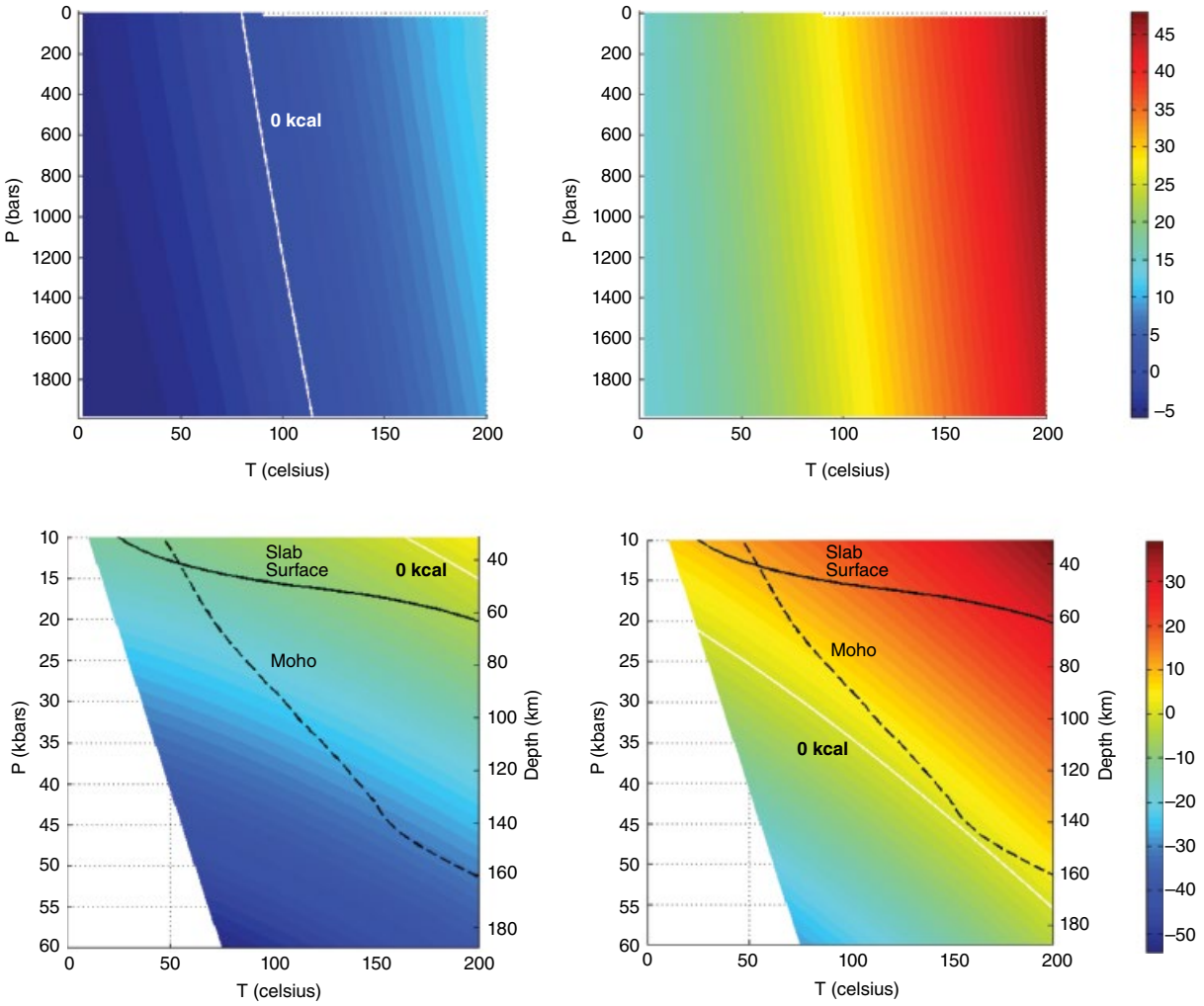

Figure 25.8 Color maps of affinity (in kcal mol^{-1}) across temperature and pressure for the overall forward citric acid cycle as written in Box 25.1 at both low-pressure (top) and high-pressure conditions. In each pressure version, the minimum affinity values are shown on the left and maximum affinity values on the right. High-pressure plots contain slab-surface and Moho trajectories for the Tonga subduction zone from Figure 25.5. Equilibrium contours, where A = 0, are shown by the white lines. At conditions where A > 0, energy would be released by running the citric acid cycle in the forward direction, and where A < 0, energy would be released by running the cycle in the reverse direction. Note the shift in location for the A = 0 contour between the minimum and maximum affinity plots at higher pressures. See electronic version for color representation of the figures in this book.

25.6. CONCLUDING REMARKS

Uncertainties in the internal compositions of microbial cells inhibit full assessments of affinities for the citric acid cycle and its individual steps throughout the deep biosphere. We have tried to limit ambiguity by selecting a single set of compositions for most of the compounds in the cycle. At the same time, we allowed activities of H_2(aq) and CO_2(aq) to vary in response to plausible ranges of geochemical compositions. These uncharged solutes are likely to diffuse more easily across cell membranes than ions, which means their activities can be imposed on microbial cells from external geochemical processes. The inescapable influence of external processes on these constituents of the citric acid cycle raises the possibility that geochemical processes can determine whether energy is released as the citric acid cycle operates in either the forward or reverse directions in the deep biosphere.

We find from this analysis that our proposal that conditions in shallow ranges of subduction zones may be conducive to life is tenable. The deep biosphere may indeed extend much further into the subsurface than we presently have access. There is even the possibility that these results could refresh thinking about early life on Earth. Genetic evidence from all known life sends a strong message that use of chemical energy sources

preceded the use of sunlight to power life on Earth (Shock & Boyd, 2015). The inescapable conclusion from this existing evidence is that there is no compelling reason to think that life emerged at the surface or that early habitats should be equated to those at the surface. Instead, life itself seems to indicate that it had geologic origins that were plausibly internal to the planet. The energetic analysis performed in this study shows that one of the central biochemical cycles that is deeply engrained in biological energy transfer may be intimately tied to geochemical compositions that can vary enormously with depth.

We anticipate that calculations of this kind can be improved upon. Here are some ways:

• The main source of constraints for the abundances of compounds involved in the citric acid cycle is studies of *Escherichia coli*, which is hardly a denizen of the deep biosphere. Perhaps the ongoing metabolomic revolution will provide economical ways to inventory internal cellular compositions of a wider variety of microbes, including deep residents. The results could be used in a far more comprehensive analysis of how compositions affect affinities and therefore the directions that the citric acid cycle can be run for an energetic profit in subsurface habitats, and the magnitudes of those energy releases. Additional advances in theoretical estimations could open other biochemical pathways to investigation.

• Subsurface exploration for life can expand through scientific drilling, especially if those drilling efforts focus on extreme conditions in the accessible subsurface that may be most similar to those that persist in the far less accessible reaches of subduction zones that may indeed be habitable. Intensive sampling and analysis of subsurface fluids for inorganic and organic solutes, together with live capture of subsurface residents, will improve the compositional framework adopted here.

• The standard state properties for the citric acid cycle used here come from our critique of the available data (Canovas & Shock, 2016), and we refer to the review there for extensive and obvious gaps in current knowledge. While we are optimistic that our predictions are applicable to high pressure and temperature extremes of the biosphere, we would also not be surprised to find that crucial refinements are possible. Specifically, measurements of partial molar properties of solutes involved in the citric acid cycle at high temperatures and pressures would revolutionize the accuracy of predictions of the type attempted here.

• We adopted pressure-temperature-depth relations for the Tonga subduction zone because it is steep, which allows subducted materials to reach high pressures while still in the relatively low temperature range compatible with known life. Other pressure-temperature-depth models are likely to lead to other conclusions about how chemical energy can be accessed through the citric acid cycle in other specific locations.

ACKNOWLEDGMENTS

We thank Tucker Ely, Grayson Boyer, Alta Howells, Kirt Robinson, Kris Fecteau, Chris Glein, Kristin Johnson, Meghan Guild, Dimitri Sverjensky, and Eric Boyd for helpful conversations during the course of this research. This work was supported by grants from the Sloan Foundation to the Extreme Chemistry and Physics community of the Deep Carbon Observatory. Particular thanks are owed to Craig Manning and Wendy Mao for their patience while we prepared the results of this study for publication.

REFERENCES

Amend, J. P., & Shock, E. L. (2001). Energetics of overall metabolic reactions of thermophilic and hyperthermophilic Archaea and Bacteria. *FEMS Microbiology Reviews*, *25*(2), 175–243.

Apps, J. (2010). Geohydrological studies for nuclear waste isolation at the Hanford Reservation: Vol. I. Executive summary; Vol. II. Final report. *Lawrence Berkeley National Laboratory*.

Arcuri, E. J., & Ehrlich, H. L. (1977). Influence of hydrostatic pressure on the effects of the heavy metal cations of manganese, copper, cobalt, and nickel on the growth of three deep-sea bacterial isolates. *Applied and Environmental Microbiology*, *33*(2), 282–288.

Ask, D., Stephansson, O., & Cornet, F.H. (2001). Integrated stress analysis of hydraulic stress data in the Äspö region, Sweden. Analysis of hydraulic fracturing stress data and hydraulic tests on pre-existing fractures (HTPF) in boreholes KAS02, KAS03, and KLX02. *SKB International Progress Report*, IPR-01-26, Stockholm.

Bakermans, C., Ayala-del-Río, H. L., Ponder, M. A., Vishnivetskaya, T., Gilichinsky, D., Thomashow, M. F., & Tiedje, J. M. (2006). *Psychrobacter cryohalolentis* sp. nov. and *Psychrobacter arcticus* sp. nov., isolated from Siberian permafrost. *International Journal of Systematic and Evolutionary Microbiology*, *56*(6), 1285–1291.

Bale, S. J., Goodman, K., Rochelle, P. A., Marchesi, J. R., Fry, J. C., Weightman, A. J., & Parkes, R. J. (1997). *Desulfovibrio profundus* sp. nov., a novel barophilic sulfate-reducing bacterium from deep sediment layers in the Japan Sea. *International Journal of Systematic Bacteriology*, *47*(2), 515–521.

Bartlett, D. H. (2002). Pressure effects on in vivo microbial processes. *Biochimica et Biophysica Acta (BBA)-Protein Structure and Molecular Enzymology*, *1595*(1), 367–381.

Bennett, B. D., Kimball, E. H., Gao, M., Osterhout, R., Van Dien, S. J., & Rabinowitz, J. D. (2009). Absolute metabolite concentrations and implied enzyme active site occupancy in *Escherichia coli*. *Nature Chemical Biology*, *5*(8), 593–599.

Bernhardt, G., Jaenicke, R., Lüdemann, H. D., König, H., & Stetter, K. O. (1988). High pressure enhances the growth rate of the thermophilic archaebacterium *Methanococcus thermolithotrophicus* without extending its temperature range. *Applied and Environmental Microbiology*, *54*(5), 1258–1261.

Bonch-Osmolovskaya, E. A., Miroshnichenko, M. L., Lebedinsky, A. V., Chernyh, N. A., Nazina, T. N., Ivoilov, V.

S., et al. (2003). Radioisotopic, culture-based, and oligonucleotide microchip analyses of thermophilic microbial communities in a continental high-temperature petroleum reservoir. *Applied and Environmental Microbiology*, *69*(10), 6143–6151.

Böning, P., Brumsack, H. J., Böttcher, M. E., Schnetger, B., Kriete, C., Kallmeyer, J., & Borchers, S. L. (2004). Geochemistry of Peruvian near-surface sediments. *Geochimica et Cosmochimica Acta*, *68*(21), 4429–4451.

Brazelton, W. J., & Baross, J. A. (2009). Abundant transposases encoded by the metagenome of a hydrothermal chimney biofilm. *The ISME journal*, *3*(12), 1420–1424.

Breezee, J., Cady, N., & Staley, J. T. (2004). Subfreezing growth of the sea ice bacterium "*Psychromonas ingrahamii*". *Microbial Ecology*, *47*(3), 300–304.

Byers, H. K., Stackebrandt, E., Hayward, C., & Blackall, L. L. (1998). Molecular investigation of a microbial mat associated with the Great Artesian Basin. *FEMS Microbiology Ecology*, *25*(4), 391–403.

Canganella, F., Gonzalez, J. M., Yanagibayashi, M., Kato, C., & Horikoshi, K. (1997). Pressure and temperature effects on growth and viability of the hyperthermophilic archaeon *Thermococcus peptonophilus*. *Archives of Microbiology*, *168*(1), 1–7.

Canovas, P. C. III, & Shock, E. L. (2016). Geobiochemistry of metabolism: Standard state thermodynamic properties of the citric acid cycle. *Geochimica et Cosmochimica Acta*, *195*, 293–322.

Carvalho, V.M.L. (2013). Metagenomic Analysis of Mariana Trench Sediment Samples. Master's thesis, University of Copenhagen.

Charlou, J. L., Donval, J. P., Fouquet, Y., Jean-Baptiste, P., & Holm, N. (2002). Geochemistry of high H_2 and CH_4 vent fluids issuing from ultramafic rocks at the Rainbow hydrothermal field (36° 14′ N, MAR). *Chemical Geology*, *191*(4), 345–359.

Chivian, D., Brodie, E. L., Alm, E. J., Culley, D. E., Dehal, P. S., DeSantis, T. Z., et al. (2008). Environmental genomics reveals a single-species ecosystem deep within Earth. *Science*, *322*(5899), 275–278.

Collins, R. E., Rocap, G., & Deming, J. W. (2010). Persistence of bacterial and archaeal communities in sea ice through an Arctic winter. *Environmental Microbiology*, *12*(7), 1828–1841.

Colman, D. R., Poudel, S., Stamps, B.W., Boyd, E. S., & Spear J. R. (2017). The deep, hot biosphere: Twenty-five years of retrospection. *Proceedings of the National Academy of Sciences*, *114*(27), 6895–6903.

Daumas, S., Cord-Ruwisch, R., & Garcia, J. L. (1988). *Desulfotomaculum geothermicum* sp. nov., a thermophilic, fatty acid-degrading, sulfate-reducing bacterium isolated with H_2 from geothermal ground water. *Antonie van Leeuwenhoek*, *54*(2), 165–178.

Daumas, S., Lombart, R., & Bianchi, A. (1986). A bacteriological study of geothermal spring waters dating from the Dogger and Trias period in the Paris basin. *Geomicrobiology Journal*, *4*(4), 423–433.

D'Elia, T., Veerapaneni, R., & Rogers, S. O. (2008). Isolation of microbes from Lake Vostok accretion ice. *Applied and Environmental Microbiology*, *74*(15), 4962–4965.

DeLong, E. F., Franks, D. G., & Yayanos, A. A. (1997). Evolutionary relationships of cultivated psychrophilic and barophilic deep-sea bacteria. *Applied and Environmental Microbiology*, *63*(5), 2105–2108.

Delwiche, M., Colwell, F. S., Tseng, H.-Y., Gao, G., & Onstott, T. C. (1996). Pressure and temperature adaptation of a bacterium recovered from 2.8 kilometers beneath the surface of the earth. Abstr. 96th Annual Meeting American Society for Microbiology, New Orleans.

Deming, J. W., & Baross, J. A. (1986). Solid medium for culturing black smoker bacteria at temperatures to 120 °C. *Applied and Environmental Microbiology*, *51*(2), 238–243.

Deming, J. W., Somers, L. K., Straube, W. L., Swartz, D. G., & Macdonell, M. T. (1988). Isolation of an obligately barophilic bacterium and description of a new genus, *Colwellia* gen. nov. *Systematic and Applied Microbiology*, *10*(2), 152–160.

Ehrlich, H. L., Ghiorse, W. C., & Johnson G. L. (1972). Distribution of microbes in manganese modules from the Atlantic and Pacific oceans. *Developments in Industrial Microbiology*, *13*, 57–65.

Ekendahl, S., & Pedersen, K. (1994). Carbon transformations by attached bacterial populations in granitic groundwater from deep crystalline bed-rock of the Stripa research mine. *Microbiology*, *140*(7), 1565–1573.

Ellis, W. L., & Ege, J. R. (1975). Determination of *in situ* stress in U12g tunnel, Rainier Mesa, Nevada Test Site, Nevada. *U.S. Geological Survey Report RSGS* 474–219, 18 p.

Erauso, G., Reysenbach, A. L., Godfroy, A., Meunier, J. R., Crump, B., Partensky, F., et al. (1993). *Pyrococcus abyssi* sp. nov., a new hyperthermophilic archaeon isolated from a deep-sea hydrothermal vent. *Archives of Microbiology*, *160*(5), 338–349.

Facq, S., Daniel, I., Montagnac, G., Carbon, H., & Sverjensky, D. A. (2014). *In situ* Raman study and thermodynamic model of aqueous carbonate speciation in equilibrium with aragonite under subduction zone conditions. *Geochimica et Cosmochimica Acta*, *132*, 375–390.

Fardeau, M. L., Magot, M., Patel, B. K., Thomas, P., Garcia, J. L., & Ollivier, B. (2000). *Thermoanaerobacter subterraneus* sp. nov., a novel thermophile isolated from oilfield water. *International Journal of Systematic and Evolutionary Microbiology*, *50*(6), 2141–2149.

Fell, J. W. (1967) Distribution of yeasts in the Indian Ocean. *Bull. Mar. Sci.*, *17*, 454–470.

Grabowski, A., Tindall, B. J., Bardin, V., Blanchet, D., & Jeanthon, C. (2005). *Petrimonas sulfuriphila* gen. nov., sp. nov., a mesophilic fermentative bacterium isolated from a biodegraded oil reservoir. *International Journal of Systematic and Evolutionary Microbiology*, *55*(3), 1113–1121.

Greene, A. C., Patel, B. K., & Sheehy, A. J. (1997). *Deferribacter thermophilus* gen. nov., sp. nov., a novel thermophilic manganese- and iron-reducing bacterium isolated from a petroleum reservoir. *International Journal of Systematic Bacteriology*, *47*(2), 505–509.

Grossman, D., & Shulman, S. (1995). The biosphere below. *Earth (Waukesha, Wis.)*, *4*(3), 34–40.

Guild, M., & Shock, E. L. (2019). Carbon speciation in subduction zone fluids. In W. Mao & C. Manning (Eds.), *Deep Carbon* (this volume).

Haldeman, D. L., Amy, P. S., Ringelberg, D., & White, D. C. (1993). Characterization of the microbiology within a 21 m^3 section of rock from the deep subsurface. *Microbial Ecology*, *26*(2), 145–159.

Havig, J. R., Raymond, J., Meyer-Dombard, D. R., Zolotova, N., & Shock E. L. (2011). Merging isotopes and community genomics in a siliceous sinter-depositing hot spring, *Journal of Geophysical Research*, *116*, G01005, doi:10.1029/2010JG001415.

Helgeson, H. C. (1979) Mass transfer among minerals and hydrothermal solutions. In H. L. Barnes (Ed.), *Geochemistry of Hydrothermal Ore Deposits* (pp. 568–610). New York: John Wiley.

Hoshino, T., & Inagaki, F. (2019). Abundance and distribution of Archaea in the subseafloor sedimentary biosphere. *The ISME Journal*, *13*, 227–231.

Huang, F., Daniel, I., Cardon, H., Montagnac, G., & Sverjensky D. A. (2017). Immiscible hydrocarbon fluids in the deep carbon cycle. *Nature Communications*, *8*, 15798. https://doi.org/10.1038/ncomms15798

Inagaki, F., Hinrichs, K.-U., Kubo, Y. Bowles, M. W., Heuer, V. B., Hong, W.-L., et al. (2015). Exploring deep microbial life in coal-bearing sediment down to ~2.5 km below the ocean floor. *Science*, *349*(6246), 420–424.

Inagaki, F., Takai, K., Hirayama, H., Yamato, Y., Nealson, K. H., & Horikoshi, K. (2003). Distribution and phylogenetic diversity of the subsurface microbial community in a Japanese epithermal gold mine. *Extremophiles*, *7*(4), 307–317.

Ino, K., Konno, U., Kouduka, M., Hirota, A., Togo, Y. S., Fukuda, A., et al. (2016). Deep microbial life in high-quality granitic groundwater from geochemically and geographically distinct underground boreholes. *Environmental Microbiology Reports*, *8*, 285–294. doi: 10.1111/1758-2229.12379

Ishii, N., Nakahigashi, K., Baba, T., Robert, M., Soga, T., Kanai, A., et al. (2007). Multiple high-throughput analyses monitor the response of *E. coli* to perturbations. *Science*, *316*(5824), 593–597.

Johnson, J. W., Oelkers, E. H., & Helgeson, H. C. (1992). SUPCRT92: A software package for calculating the standard molal thermodynamic properties of minerals, gases, aqueous species, and reactions from 1 to 5000 bar and 0 to 1000 C. *Computers & Geosciences*, *18*(7), 899–947.

Kaksonen, A. H., Plumb, J. J., Robertson, W. J., Spring, S., Schumann, P., Franzmann, P. D., & Puhakka, J. A. (2006). Novel thermophilic sulfate-reducing bacteria from a geothermally active underground mine in Japan. *Applied and Environmental Microbiology*, *72*(5), 3759–3762.

Kaksonen, A. H., Spring, S., Schumann, P., Kroppenstedt, R. M., & Puhakka, J. A. (2006). *Desulfotomaculum thermosubterraneum* sp. nov., a thermophilic sulfate-reducer isolated from an underground mine located in a geothermally active area. *International Journal of Systematic and Evolutionary Microbiology*, *56*(11), 2603–2608.

Kallmeyer, J., Pockalny, R., Adhikari, R. R., Smith, D. C., & D'Hondt, S. (2012). Global distribution of microbial abundance and biomass in sub-seafloor sediment. *Proceedings of the National Academy of Sciences*, *109*, 16213–16216.

Kato, C., Li, L., Nogi, Y., Nakamura, Y., Tamaoka, J., & Horikoshi, K. (1998). Extremely barophilic bacteria isolated from the Mariana Trench, Challenger Deep, at a depth of 11,000 meters. *Applied and Environmental Microbiology*, *64*(4), 1510–1513.

Kato, C., Li, L., Tamaoka, J., & Horikoshi, K. (1997). Molecular analyses of the sediment of the 11000-m deep Mariana Trench. *Extremophiles*, *1*(3), 117–123.

Kato, C., Masui, N., & Horikoshi, K. (1996). Properties of obligately barophilic bacteria isolated from a sample of deep-sea sediment from the Izu-Bonin Trench, *Journal of Marine Biotechnology*, *4*, 96–99.

Kato, C., Sato, T., & Horikoshi, K. (1995). Isolation and properties of barophilic and barotolerant bacteria from deep-sea mud samples. *Biodiversity & Conservation*, *4*(1), 1–9.

Kieft, T. L., Fredrickson, J. K., Onstott, T. C., Gorby, Y. A., Kostandarithes, H. M., Bailey, T. J., et al. (1999). Dissimilatory reduction of Fe (III) and other electron acceptors by a Thermus isolate. *Applied and Environmental Microbiology*, *65*(3), 1214–1221.

Kieft, T. L., McCuddy, S. M., Onstott, T. C., Davidson, M., Lin, L. H., Mislowack, B., et al. (2005). Geochemically generated, energy-rich substrates and indigenous microorganisms in deep, ancient groundwater. *Geomicrobiology Journal*, *22*(6), 325–335.

Kimura, H., Sugihara, M., Yamamoto, H., Patel, B. K., Kato, K., & Hanada, S. (2005). Microbial community in a geothermal aquifer associated with the subsurface of the Great Artesian Basin, Australia. *Extremophiles*, *9*(5), 407–414.

Klouche, N., Fardeau, M. L., Lascourrèges, J. F., Cayol, J. L., Hacene, H., Thomas, P., & Magot, M. (2007). *Geosporobacter subterraneus* gen. nov., sp. nov., a spore-forming bacterium isolated from a deep subsurface aquifer. *International Journal of Systematic and Evolutionary Microbiology*, *57*(8), 1757–1761.

Kotelnikova, S., Macario, A. J., & Pedersen, K. (1998). *Methanobacterium subterraneum* sp. nov., a new alkaliphilic, eurythermic and halotolerant methanogen isolated from deep granitic groundwater. *International Journal of Systematic Bacteriology*, *48*(2), 357–367.

Kotelnikova, S., & Pedersen, K. (1998). Microbial oxygen consumption in Äspö tunnel environment, SKB-PR-HRL-98-1, Swedish Nuclear Fuel Waste Management Company, Stockholm, Sweden.

Kotlar, H. K., Lewin, A., Johansen, J., Throne-Holst, M., Haverkamp, T., Markussen, S., et al. (2011). High coverage sequencing of DNA from microorganisms living in an oil reservoir 2.5 kilometres subsurface. *Environmental Microbiology Reports*, *3*(6), 674–681.

LaRowe, D. E., & Helgeson, H. C. (2006a). Biomolecules in hydrothermal systems: Calculation of the standard molal thermodynamic properties of nucleic-acid bases, nucleosides, and nucleotides at elevated temperatures and pressures. *Geochimica et Cosmochimica Acta*, *70*, 4680–4724.

LaRowe, D. E. & Helgeson, H. C. (2006b). The energetics of metabolism in hydrothermal systems: Calculation of the standard molal thermodynamic properties of magnesium complexed adenosine nucleotides and NAD and NADP at elevated temperatures and pressures. *Thermochimica Acta*, *448*, 82–106.

L'Haridon, S., Reysenbach, A. L., Glenat, P., Prieur, D., & Jeanthon, C. (1995). Hot subterranean biosphere in a continental oil reservoir. *Nature*, *377*(6546), 223–224.

Li, H., Yang, S. Z., Mu, B. Z., Rong, Z. F., & Zhang, J. (2006). Molecular analysis of the bacterial community in a continental high-temperature and water-flooded petroleum reservoir. *FEMS Microbiology Letters*, *257*(1), 92–98.

Li, H., Yang, S. Z., Mu, B. Z., Rong, Z. F., & Zhang, J. (2007). Molecular phylogenetic diversity of the microbial community associated with a high-temperature petroleum reservoir at an offshore oilfield. *FEMS Microbiology Ecology*, *60*(1), 74–84.

Li, X. L., Bastiaens, W., Van Marcke, P., Verstricht, J., Chen, G. J., Weetjens, E., & Sillen, X. (2010). Design and development of large-scale in-situ PRACLAY heater test and horizontal high-level radioactive waste disposal gallery seal test in Belgian HADES. *Journal of Rock Mechanics and Geotechnical Engineering*, *2*(2), 103–110.

Liesack, W., Weyland, H., & Stackebrandt, E. (1991). Potential risks of gene amplification by PCR as determined by 16S rDNA analysis of a mixed-culture of strict barophilic bacteria. *Microbial Ecology*, *21*(1), 191–198.

Liu, Y., Karnauchow, T. M., Jarrell, K. F., Balkwill, D. L., Drake, G. R., Ringelberg, D., Clarno, R. & Boone, D. R. (1997). Description of two new thermophilic *Desulfotomaculum* spp., *Desulfotomaculum putei* sp. nov., from a deep terrestrial subsurface, and *Desulfotomaculum luciae* sp. nov., from a hot spring. *International Journal of Systematic and Evolutionary Microbiology*, *47*(3), 615–621.

Loiacono, S. T., Meyer-Dombard, D.A.R., Havig, J. R., Poret-Peterson, A. T., Hartnett, H. E., & Shock, E. L. (2012). Evidence for high-temperature in situ nifH transcription in an alkaline hot spring of Lower Geyser Basin, Yellowstone National Park. *Environmental Microbiology*, *14*(5), 1272–1283.

Love, C. A., Patel, B.K.C., Nichols, P. D., & Stackebrandt, E. (1993). *Desulfotomaculum australicum*, sp. nov., a thermophilic sulfate-reducing bacterium isolated from the Great Artesian Basin of Australia. *Systematic and Applied Microbiology*, *16*(2), 244–251.

Lu, S., Eiteman, M. A., & Altman, E. (2009). Effect of CO_2 on succinate production in dual-phase *Escherichia coli* fermentations. *Journal of Biotechnology*, *143*(3), 213–223.

Magnabosco, C., Lin, L.-H., Dong, H., Bomberg, M., Ghiorse, W., Stan-Lotter, H., et al. (2018). The biomass and biodiversity of the continental subsurface. *Nature Geoscience*, *11*, 707–717.

Marteinsson, V. T., Birrien, J. L., Reysenbach, A. L., Vernet, M., Marie, D., Gambacorta, A., et al. (1999). *Thermococcus barophilus* sp. nov., a new barophilic and hyperthermophilic archaeon isolated under high hydrostatic pressure from a deep-sea hydrothermal vent. *International Journal of Systematic and Evolutionary Microbiology*, *49*(2), 351–359.

Marteinsson, V. T., Moulin, P., Birrien, J., Gambacorta, A., Vernet, M., & Prieur, D. (1997). Physiological responses to stress conditions and barophilic behavior of the hyperthermophilic vent archaeon *Pyrococcus abyssi*. *Applied and Environmental Microbiology*, *63*(4), 1230–1236.

Marteinsson, V. T., Runarsson, A., Stefánsson, A., Thorsteinsson, T., Johannesson, T., Magnusson, S. H., et al. (2013). Microbial communities in the subglacial waters of the Vatnajökull ice cap, Iceland. *The ISME Journal*, *7*(2), 427–437.

McCollom, T. (2007) Geochemical constraints on sources of metabolic energy for chemolithoautotrophy in ultramafic-hosted deep-sea hydrothermal systems. *Astrobiology*, *7*, 933–950.

Meersman, F., Daniel, I., Bartlett, D. H., Winter, R., Hazel, R., & McMillan, P. F. (2013). High-pressure biochemistry and biophysics. *Reviews in Mineralogy and Geochemistry*, *75*, 607–648.

Merlin, C., Masters, M., McAteer, S., & Coulson, A. (2003). Why is carbonic anhydrase essential to *Escherichia coli*? *Journal of Bacteriology*, *185*(21), 6415–6424.

Meyer-Dombard, D.A.R., Swingley, W., Raymond, J., Havig, J., Shock, E. L., & Summons, R. E. (2011). Hydrothermal ecotones and streamer biofilm communities in the Lower Geyser Basin, Yellowstone National Park. *Environmental Microbiology*, *13*(8), 2216–2231.

Miller, J. F., Shah, N. N., Nelson, C. M., Ludlow, J. M., & Clark, D. S. (1988). Pressure and temperature effects on growth and methane production of the extreme thermophile *Methanococcus jannaschii*. *Applied and Environmental Microbiology*, *54*(12), 3039–3042.

Miyoshi, T., Iwatsuki, T., & Naganuma, T. (2005). Phylogenetic characterization of 16S rRNA gene clones from deep-groundwater microorganisms that pass through 0.2-micrometer-pore-size filters. *Applied and Environmental Microbiology*, *71*(2), 1084–1088.

Mochimaru, H., Yoshioka, H., Tamaki, H., Nakamura, K., Kaneko, N., Sakata, S., Imachi, H., Sekiguchi, Y., Uchiyama, H. & Kamagata, Y. (2007). Microbial diversity and methanogenic potential in a high temperature natural gas field in Japan. *Extremophiles*, *11*(3), 453–461.

Mori, K., Hanada, S., Maruyama, A., & Marumo, K. (2002). *Thermanaeromonas toyohensis* gen. nov., sp. nov., a novel thermophilic anaerobe isolated from a subterranean vein in the Toyoha Mines. *International Journal of Systematic and Evolutionary Microbiology*, *52*(5), 1675–1680.

Morita, R. Y., & ZoBell, C. E. (1955). Occurrence of bacteria in pelagic sediments collected during the Mid-Pacific Expedition. *Deep Sea Research (1953)*, *3*(1), 66–73.

Motamedi, M., & Pedersen, K. (1998). Note on *Desulfovibrio aespoeensis* sp. nov., a mesophilic sulfate-reducing bacterium from deep groundwater at Äspö hard rock laboratory, Sweden. *International Journal of Systematic Bacteriology*, *48*(1), 311–315.

Nakai R., Abe T., Takeyama H., & Naganuma T. (2011). Metagenomic analysis of 0.2-mm-passable microorganisms in deep-sea hydrothermal fluid. *Marine Biotechnology*, *13*, 900–908.

Nazina, T. N., Grigor'Yan, A. A., Shestakova, N. M., Babich, T. L., Ivoilov, V. S., Feng, Q., et al. (2007). Microbiological investigations of high-temperature horizons of the Kongdian petroleum reservoir in connection with field trial of a biotechnology for enhancement of oil recovery. *Microbiology*, *76*(3), 287–296.

Nilsen, R. K., & Torsvik, T. (1996). *Methanococcus thermolithotrophicus* isolated from North Sea oil field reservoir water. *Applied and Environmental Microbiology*, *62*(2), 728–731.

Nilsen, R. K., Beeder, J., Thorstenson, T., & Torsvik, T. (1996). Distribution of thermophilic marine sulfate reducers in

North Sea oil field waters and oil reservoirs. *Applied and Environmental Microbiology*, *62*(5), 1793–1798.

Nilsen, R. K., Torsvik, T., & Lien, T. (1996). *Desulfotomaculum thermocisternum* sp. nov., a sulfate reducer isolated from a hot North Sea oil reservoir. *International Journal of Systematic Bacteriology*, *46*(2), 397–402.

Nogi, Y., Masui, N., & Kato, C. (1998). *Photobacterium profundum* sp. nov., a new, moderately barophilic bacterial species isolated from a deep-sea sediment. *Extremophiles*, *2*(1), 1–8.

Nunoura, T., Hirayama, H., Takami, H., Oida, H., Nishi, S., Shimamura, S., et al. (2005). Genetic and functional properties of uncultivated thermophilic crenarchaeotes from a subsurface gold mine as revealed by analysis of genome fragments. *Environmental Microbiology*, *7*(12), 1967–1984.

Olson, G. J., Dockins, W. S., McFeters, G. A., & Iverson, W. P. (1981). Sulfate-reducing and methanogenic bacteria from deep aquifers in Montana. *Geomicrobiology Journal*, *2*(4), 327–340.

Onstott, T. C., Phelps, T. J., Colwell, F. S., Ringelberg, D., White, D. C., Boone, D. R., et al. (1998). Observations pertaining to the origin and ecology of microorganisms recovered from the deep subsurface of Taylorsville Basin, Virginia. *Geomicrobiology Journal*, *15*(4), 353–385.

Onstott, T. C., Tobin, K., Dong, H., DeFlaun, M. F., Fredrickson, J. K., Bailey, T., et al. (1997). Deep gold mines of South Africa: Windows into the subsurface biosphere. *Optical Science, Engineering and Instrumentation '97* (344–357). International Society for Optics and Photonics.

Panikov, N. S., & Sizova, M. V. (2007). Growth kinetics of microorganisms isolated from Alaskan soil and permafrost in solid media frozen down to −35 C. *FEMS Microbiology Ecology*, *59*(2), 500–512.

Parkes, R. J., Cragg, B. A., Bale, S. J., Getliff, J. M., Goodman, K., Rochelle, P. A., et al. (1994). Deep bacterial biosphere in Pacific Ocean sediments. *Nature*, *371*(6496), 410–413.

Pedersen, K. (1997). Microbial life in deep granitic rock. *FEMS Microbiology Reviews*, *20*(3-4), 399–414.

Pedersen, K., & Ekendahl, S. (1990). Distribution and activity of bacteria in deep granitic groundwaters of southeastern Sweden. *Microbial Ecology*, *20*(1), 37–52.

Peng, L., Arauzo-Bravo, M. J., & Shimizu, K. (2004). Metabolic flux analysis for a ppc mutant *Escherichia coli* based on ^{13}C-labelling experiments together with enzyme activity assays and intracellular metabolite measurements. *FEMS Microbiology Letters*, *235*(1), 17–23.

Phillips, R., Kondev, J., Theriot, J., & Garcia, H. (2008). *Physical Biology of the Cell*. New York: Garland Science.

Pope, D. H., Smith, W. P., Swartz, R. W., & Landau, J. V. (1975). Role of bacterial ribosomes in barotolerance. *Journal of Bacteriology*, *121*, 664–669.

Price, P. B., & Sowers, T. (2004). Temperature dependence of metabolic rates for microbial growth, maintenance, and survival. *Proceedings of the National Academy of Sciences of the United States of America*, *101*(13), 4631–4636.

Rivkina, E. M., Friedmann, E. I., McKay, C. P., & Gilichinsky, D. A. (2000). Metabolic activity of permafrost bacteria below the freezing point. *Applied and Environmental Microbiology*, *66*(8), 3230–3233.

Rosnes, J. T., Torsvik, T., & Lien, T. (1991). Spore-forming thermophilic sulfate-reducing bacteria isolated from North Sea oil field waters. *Applied and Environmental Microbiology*, *57*(8), 2302–2307.

Russell, C. E., Jacobson, R., Haldeman, D. L., & Amy, P. S. (1994). Heterogeneity of deep subsurface microorganisms and correlations to hydrogeological and geochemical parameters. *Geomicrobiology Journal*, *12*(1), 37–51.

Sahl, J. W., Schmidt, R., Swanner, E. D., Mandernack, K. W., Templeton, A. S., Kieft, T. L., et al. (2008). Subsurface microbial diversity in deep-granitic-fracture water in Colorado. *Applied and Environmental Microbiology*, *74*(1), 143–152.

Salamatin, A. N., Lipenkov, V. Y., Barkov, N. I., Jouzel, J., Petit, J. R., & Raynaud, D. (1998). Ice core age dating and paleothermometer calibration based on isotope and temperature profiles from deep boreholes at Vostok Station (East Antarctica). *Journal of Geophysical Research: Atmospheres (1984–2012)*, *103*(D8), 8963–8977.

Salisbury, M. H., Shinohara, M., Richter, C., Araki, E., Barr, S. R., D'Antonio, M., et al. (2002). Leg 195 summary. In M. H. Salisbury, et al. (Eds.), *Proceedings of the Ocean Drilling Program, Initial Reports* (Vol. 195, pp. 1–63). College Station, Texas: Ocean Drilling Program.

Schippers, A., & Neretin, L. N. (2006). Quantification of microbial communities in near-surface and deeply buried marine sediments on the Peru continental margin using real-time PCR. *Environmental Microbiology*, *8*(7), 1251–1260.

Scholander, P. F., Bradstreet, E. D., Hemmingsen, E. A., & Hammel, H. T. (1965). Sap pressure in vascular plants: Negative hydrostatic pressure can be measured in plants. *Science*, *148*(3668), 339–346.

Schwarz, J. R., & Colwell, R. R. (1975a). Macromolecular biosynthesis in Pseudomonas bathycetes at deep-sea pressure and temperature. In Proceedings, 75th annual meeting of the American Society for Microbiology, American Society for Microbiology, Washington DC, p. 162.

Schwarz, J. R., & Colwell, R. R. (1975b). Heterotrophic activity of deep-sea sediment bacteria. *Applied Microbiology*, *30*(4), 639–649.

Schwarz, J. R., Walker, J. D., & Colwell, R. R. (1975). Deep-sea bacteria: Growth and utilization of n-hexadecane at in situ temperature and pressure. *Canadian Journal of Microbiology*, *21*(5), 682–687.

Sharma, A., Scott, J. H., Cody, G. D., Fogel, M. L., Hazen, R. M., Hemley, R. J., & Huntress, W. T. (2002). Microbial activity at gigapascal pressures. *Science*, *295*(5559), 1514–1516.

Shi, T., Reeves, R. H., Gilichinsky, D. A., & Friedmann, E. I. (1997). Characterization of viable bacteria from Siberian permafrost by 16S rDNA sequencing. *Microbial Ecology*, *33*(3), 169–179.

Shock, E. L. (2009). Minerals as energy sources for microorganisms. *Economic Geology*, *104*(8), 1235–1248

Shock, E. L., & Boyd, E. S. (2015). Principles of geobiochemistry. *Elements*, *11*, 395–401.

Shock, E. L., & Canovas, P. C. (2010). The potential for abiotic organic synthesis and biosynthesis at seafloor hydrothermal systems. *Geofluids*, *10*, 161–192.

Shock, E. L., Oelkers, E. H., Johnson, J. W., Sverjensky, D. A., & Helgeson, H. C. (1992). Calculation of the thermodynamic properties of aqueous species at high pressures and temperatures: Effective electrostatic radii, dissociation constants, and

standard partial molal properties to 1000 °C and 5 kb. *Journal of the Chemical Society, Faraday Transactions*, *88*, 803–826.

Stetter, K. O., Huber, R., Blöchl, E., Kurr, M., Eden, R. D., Fielder, M., et al. (1993). Hyperthermophilic archaea are thriving in deep North Sea and Alaskan oil reservoirs. *Nature*, *365*(6448), 743–745.

Steurer, J. F., & Underwood, M. B. (2003). Data report: The relation between physical properties and grain-size variations in hemipelagic sediments from Nankai Trough. In *Proceedings of the Ocean Drilling Program, Scientific Results*, *190*(196), 1–25.

Stevens, T. O., & McKinley, J. P. (1995). Lithoautotrophic microbial ecosystems in deep basalt aquifers. *Science*, *270*(5235), 450–455.

Stevens, T. O., McKinley, J. P., & Fredrickson, J. K. (1993). Bacteria associated with deep, alkaline, anaerobic groundwaters in southeast Washington. *Microbial Ecology*, *25*(1), 35–50.

Sundararaj, S., Guo, A., Habibi-Nazhad, B., Rouani, M., Stothard, P., Ellison, M., & Wishart, D. S. (2004). The Cybercell Database (CCDB): A comprehensive, self-updating, relational database to coordinate and facilitate *in silico* modeling of *Escherichia coli*. *Nucleic Acids Research*, *32*(Database issue), D293–D295.

Sverjensky, D. A., Harrison, B., & Azzolini, D. (2014). Water in the deep Earth: The dielectric constant and the solubilities of quartz and corundum. *Geochimica et Cosmochimica Acta*, *129*, 125–145.

Sverjensky, D. A., Stagno, V., & Huang, F. (2014). Important role of organic carbon in subduction-zone fluids in the deep carbon cycle. *Nature Geoscience*, *7*, 9–13.

Syracuse, E. M., van Keken, P. E., & Abers, G. A. (2010). The global range of subduction zone thermal models. *Physics of the Earth and Planetary Interiors*, *183*(1), 73–90.

Szewzyk, U., Szewzyk, R., & Stenström, T. A. (1994). Thermophilic, anaerobic bacteria isolated from a deep borehole in granite in Sweden. *Proceedings of the National Academy of Sciences*, *91*(5), 1810–1813.

Szewzyk, U., Szewzyk, R., & Stenstroem, T. A. (1997). Thermophilic fermentative bacteria from a deep borehole in granitic rock in Sweden. In *Optical Science, Engineering and Instrumentation '97* (pp. 330–334). International Society for Optics and Photonics.

Takai, K., Hirayama, H., Sakihama, Y., Inagaki, F., Yamato, Y., & Horikoshi, K. (2002). Isolation and metabolic characteristics of previously uncultured members of the order Aquificales in a subsurface gold mine. *Applied and Environmental Microbiology*, *68*(6), 3046–3054.

Takai, K., Moser, D. P., DeFlaun, M., Onstott, T. C., & Fredrickson, J. K. (2001). Archaeal diversity in waters from deep South African gold mines. *Applied and Environmental Microbiology*, *67*(12), 5750–5760.

Takai, K., Moser, D. P., Onstott, T. C., Spoelstra, N., Pfiffner, S. M., Dohnalkova, A., & Fredrickson, J. K. (2001). *Alkaliphilus transvaalensis* gen. nov., sp. nov., an extremely alkaliphilic bacterium isolated from a deep South African gold mine. *International Journal of Systematic and Evolutionary Microbiology*, *51*(4), 1245–1256.

Takai, K., Moyer, C. L., Miyazaki, M., Nogi, Y., Hirayama, H., Nealson, K. H., & Horikoshi, K. (2005). *Marinobacter alkaliphilus* sp. nov., a novel alkaliphilic bacterium isolated from subseafloor alkaline serpentine mud from Ocean Drilling Program Site 1200 at South Chamorro Seamount, Mariana Forearc. *Extremophiles*, *9*(1), 17–27.

Takai, K., Nakamura, K., Toki, T., Tsunogai, U., Miyazaki, M., Miyazaki, J., et al. (2008). Cell proliferation at 122 °C and isotopically heavy CH_4 production by a hyperthermophilic methanogen under high-pressure cultivation. *Proceedings of the National Academy of Sciences*, *105*(31), 10949–10954.

Tanaka, T., Burgess, J., & Wright, P. (2001). High-pressure adaptation by salt stress in a moderately halophilic bacterium obtained from open seawater. *Applied Microbiology and Biotechnology*, *57*(1–2), 200–204.

Tao, R., Zhang, L., Tian, M., Zhu, J., Liu, X., Liu, J., et al. (2018). Formation of abiotic hydrocarbon from reduction of carbonate in subduction zones: Constraints from petrological observation and experimental simulation. *Geochimica et Cosmochimica Acta*, *239*, 390–408.

Tardy-Jacquenod, C., Magot, M., Patel, B.K.C., Matheron, R., & Caumette, P. (1998). *Desulfotomaculum halophilum* sp. nov., a halophilic sulfate-reducing bacterium isolated from oil production facilities. *International Journal of Systematic Bacteriology*, *48*(2), 333–338.

Tobal, G. M. (1993). Purification and characterization of a malate dehydrogenase from the marine bacterium *Shewanella* SC2. Master's Thesis, Scripps Institute of Oceanography, University of California–San Diego, La Jolla, CA.

Trembath-Reichert, E., Morono, Y., Ijira, A., Hoshino, T., Dawson, K. S., Inagaki, F. & Orphan, V. J. (2017). Methyl-compound use and slow growth characterize microbial life in 2-km-deep subseafloor coal and shale beds. *Proceedings of the National Academy of Sciences*, *114*, E9206–E9215.

Trimarco, E., Balkwill, D., Davidson, M., & Onstott, T. C. (2006). *In situ* enrichment of a diverse community of bacteria from a 4–5 km deep fault zone in South Africa. *Geomicrobiology Journal*, *23*(6), 463–473.

Turley, C. (2000). Bacteria in the cold deep-sea benthic boundary layer and sediment–water interface of the NE Atlantic. *FEMS Microbiology Ecology*, *33*(2), 89–99.

Vanlint, D., Mitchell, R., Bailey, E., Meersman, F., McMillan, P. F., Michiels, C. W., & Aertsen, A. (2011). Rapid acquisition of gigapascal-high-pressure resistance by *Escherichia coli*. *Mbio*, *2*(1), e00130–10.

Wanger, G., Moser, D., Hay, M., Myneni, S., Onstott, T. C., & Southam, G. (2012). Mobile hydrocarbon microspheres from > 2-billion-year-old carbon-bearing seams in the South African deep subsurface. *Geobiology*, *10*(6), 496–505.

Whitman, W. B., Coleman, D. C., & Wiebe, W. J. (1998). Prokaryotes: The unseen majority. *Proceedings of the National Academy of Sciences*, *95*, 6578–6583.

Winnock, E., & Pontalier, Y. (1970). Lacq gas field, France. In *AAPG Memoir 14: Geology of Giant Petroleum Fields* (pp. 370–387). Tulsa, OK: American Association of Petroleum Geologists.

Wouters, K., Moors, H., Boven, P., & Leys, N. (2013). Evidence and characteristics of a diverse and metabolically active microbial community in deep subsurface clay borehole water. *FEMS Microbiology Ecology*, *86*(3), 458–473.

Wynter, C., Patel, B.K.C., Bain, P., Jersey, J. D., Hamilton, S., & Inkerman, P. A. (1996). A novel thermostable dextranase from a *Thermoanaerobacter* species cultured from the geothermal waters of the Great Artesian Basin of Australia. *FEMS Microbiology Letters*, *140*(2-3), 271–276.

Yanagibayashi, M., Nogi, Y., Li, L., & Kato, C. (1999). Changes in the microbial community in Japan Trench sediment from a depth of 6292 m during cultivation without decompression. *FEMS Microbiology Letters*, *170*(1), 271–279.

Yayanos, A. A. (1986). Evolutional and ecological implications of the properties of deep-sea barophilic bacteria. *Proceedings of the National Academy of Sciences*, *83*(24), 9542–9546.

Yayanos, A. A., & Dietz, A. S. (1982). Thermal inactivation of a deep-sea barophilic bacterium, isolate CNPT-3. *Applied and Environmental Microbiology*, *43*(6), 1481–1489.

Yayanos, A. A., Dietz, A. S., & Van Boxtel, R. (1981). Obligately barophilic bacterium from the Mariana Trench. *Proceedings of the National Academy of Sciences*, *78*(8), 5212–5215.

Yayanos, A. A., Dietz, A. S., & Van Boxtel, R. (1982). Dependence of reproduction rate on pressure as a hallmark of deep-sea bacteria. *Applied and Environmental Microbiology*, *44*(6), 1356–1361.

Yoshioka, H., Sakata, S., Cragg, B. A., Parkes, R. J., & Fujii, T. (2009). Microbial methane production rates in gas hydrate-bearing sediments from the eastern Nankai Trough, off central Japan. *Geochemical Journal*, *43*(5), 315–321.

Zhang, G., Dong, H., Jiang, H., Xu, Z., & Eberl, D. D. (2006). Unique microbial community in drilling fluids from Chinese continental scientific drilling. *Geomicrobiology Journal*, *23*(6), 499–514.

Zhang, G., Dong, H., Xu, Z., Zhao, D., & Zhang, C. (2005). Microbial diversity in ultra-high-pressure rocks and fluids from the Chinese Continental Scientific Drilling Project in China. *Applied and Environmental Microbiology*, *71*(6), 3213–3227.

Zimov, S. A., Schuur, E. A., & Chapin III, F. S. (2006). Permafrost and the global carbon budget. *Science*, *312*(5780), 1612–1613.

Zink, K. G., Wilkes, H., Disko, U., Elvert, M., & Horsfield, B. (2003). Intact phospholipids—microbial "life markers" in marine deep subsurface sediments. *Organic Geochemistry*, *34*(6), 755–769.

ZoBell, C. E. (1952). Bacterial life at the bottom of the Philippine Trench. *Science*, *115*(2993), 507–508.

ZoBell, C. E. (1958). Ecology of sulfate reducing bacteria. *Producers Monthly*, *22*(7), 12–29.

ZoBell, C. E., & Morita, R. Y. (1957). Barophilic bacteria in some deep sea sediments. *Journal of Bacteriology*, *73*(4), 563.